Journal of Theoretical Biology 407 (2016) 238–258

Contents lists available at ScienceDirect

Journal of Theoretical Biology

journal homepage: www.elsevier.com/locate/yjtbi

Mathematical model of galactose regulation and metabolic consumption in yeast

Tina M. Mitre [a], Michael C. Mackey [a,b,c], Anmar Khadra [a,b,c,*]

[a] Department of Mathematics, McGill University, Montreal, Quebec, Canada
[b] Department of Physiology, McGill University, Montreal, Quebec, Canada
[c] Centre for Nonlinear Dynamics, Montreal, Quebec, Canada

HIGHLIGHTS

- A new model of the genetic and metabolic branches of the GAL network is developed.
- Bistability is shown to be an inherent property of its genetic branch.
- The model is shown to be robust to genetic mutations and molecular instabilities.
- It is shown that the GAL network exhibits partial low pass filtering capacity.

ARTICLE INFO

Article history:
Received 4 February 2016
Received in revised form
1 July 2016
Accepted 4 July 2016
Available online 6 July 2016

Keywords:
Galactose gene-regulatory network
Leloir pathway
Glucose repression of galactose metabolism
Environmental adaptation
Mathematical model

ABSTRACT

The galactose network has been extensively studied at the unicellular level to broaden our understanding of the regulatory mechanisms governing galactose metabolism in multicellular organisms. Although the key molecular players involved in the metabolic and regulatory processes of this system have been known for decades, their interactions and chemical kinetics remain incompletely understood. Mathematical models can provide an alternative method to study the dynamics of this network from a quantitative and a qualitative perspective. Here, we employ this approach to unravel the main properties of the galactose network, including equilibrium binary and temporal responses, as a way to decipher its adaptation to actively-changing inputs. We combine its two main components: the genetic branch, which allows for bistable responses, and a metabolic branch, encompassing the relevant metabolic processes that can be repressed by glucose. We use both computational tools to estimate model parameters based on published experimental data, as well as bifurcation analysis to decipher the properties of the system in various parameter regimes. Our model analysis reveals that the interplay between the inducer (galactose) and the repressor (glucose) creates a bistable regime which dictates the temporal responses of the system. Based on the same bifurcation techniques, we explain why the system is robust to genetic mutations and molecular instabilities. These findings may provide experimentalists with a theoretical framework with which they can determine how the galactose network functions under various conditions.

1. Introduction

Experimental studies of genetic regulatory networks in unicellular organisms are based, at least in part, on the premise that the main regulatory mechanisms are conserved across species regardless of the complexity of the organism. The galactose network, a typical example of such a network, has been extensively studied in the budding yeast *Saccharomyces cerevisiae*. It is comprised of metabolic reactions coupled to a set of genetic regulatory processes and glucose-repressed proteins. This network is typically activated when galactose, a monosaccharide found in dairy and vegetables, becomes the only available energy source, triggering a cascade of intracellular processes that can be repressed by glucose.

The protein machinery of the galactose network comprises ~5% of the total cellular mass (Bhat, 2008). Due to this high protein load, galactose is energetically more expensive to use than glucose. As a result, cells use glucose as a transcriptional repressor of the GAL network proteins (labelled Gal proteins) when both

* Corresponding author at: Department of Physiology, McGill University, McIntyre Medical Building, 3655 Promenade Sir William Osler, Montreal, Quebec, Canada, H3G 1Y6.
E-mail address: anmar.khadra@mcgill.ca (A. Khadra).

http://dx.doi.org/10.1016/j.jtbi.2016.07.004
0022-5193/

monosaccharides (glucose and galactose) are present. Although not an essential nutrient, galactose is a crucial moiety in cellular membrane glycoproteins (de Jongh et al., 2008). Genetic mutations in the amino-acid sequence of the galactose metabolic enzymes lead to the accumulation of galactitol, an alcohol-form of galactose, to lethal levels if no food restrictions are applied. Such genetic disorders fall under the pathological condition "galactosemia", which currently affects 1 in 600,000 children (Murphy et al., 1999). Secondary effects of this disease include cataracts and neuronal degenerative disorders (Timson, 2006). For these health reasons, it is imperative to obtain a thorough understanding of the processes and pathways governing galactose regulation.

Interest in the Gal proteins first appeared in the 1940s with work by Kosterlitz (1943) that focused on galactose fermentation and metabolism in budding yeast. Mathematical modeling of this system, however, started appearing in the late 1990s with work by Venkatesh et al. (1999), focusing on the regulatory GAL network that consisted of three feedback loops. Since then, several groups have worked on variations of this study by developing models of various degrees of complexity to understand the experimental results (de Atauri et al., 2004, 2005; Ramsey et al., 2006; Acar et al., 2005, 2010; Apostu and Mackey, 2012; Venturelli et al., 2012).

For example, de Atauri and colleagues studied the effect of transcriptional noise on galactose metabolic and gene regulation by developing dynamics models of these biological systems (de Atauri et al., 2004). The models were used to explain certain aspects of the GAL network including the switch-like phenomenon, the tight control of metabolic concentrations, particularly galactose-1-phosphate (Gal1P) associated with galactosemia, and the control machinery that attenuates high-frequency noise. The control of metabolic concentrations was further analyzed to show that positive and negative regulatory feedback loops, mediated through the Gal3 and the Gal80 proteins respectively, are necessary to avoid large intracellular variations and long initial transients in the induction phase of the network (Ramsey et al., 2006). By investigating the effects of glucose oscillations, Bennett et al. (2008) then concluded that the network behaves as a low pass filter without offering a complete dynamic analysis of the properties of the system.

Examining the effect of different feedback loops through mutations in the GAL mRNA strains revealed that bistable induction curves can appear over a limited range of galactose concentrations for all yeast strains except for the GAL3 mutant, which encodes for a regulatory protein of the network (Acar et al., 2005). Interestingly, removing or diminishing various feedback loops within the system allowed for the quantification of the number of gene copies and showed the existence of a 1-to-1 stoichiometry between Gal3 and Gal80 proteins in the gene network (Acar et al., 2010).

The bistability property was further analyzed by Venturelli et al. (2012) using the GAL network model of Acar et al. (2005). The model was modified by including a simple feedback mechanism in which GAL3, GAL80 and GAL1 transcription rates depended on the Gal4 protein in a Michaelis–Menten fashion and Gal3 and Gal1 received a constant input rate upon galactose administration to the cell. It also included a recently-discovered positive feedback loop of the galactose network involving Gal1 protein (Abramczyk et al., 2012). The study demonstrated that bistability occurs due to pathways involving both Gal3 and Gal1 proteins (labelled Gal3p and Gal1p, respectively), contradicting previous experimental results by Acar et al. (2005). Moreover, it concluded that the interplay between these two positive feedback loops increases the bistability range of the system and that connections of this kind can be beneficial in nature as it may induce a faster response time to abrupt environmental changes than a single positive loop. In Apostu and Mackey (2012), the exact sequence of reactions occurring at the promoter level of GAL genes was further analyzed mathematically to determine how bistability is affected by model variations involving Gal3p, and to show that the GAL regulon is induced at the promoter level by Gal3p activated dimers through a non-dissociation sequential model.

To characterize the GAL network dynamics and to understand how various extracellular perturbations affect its memory and filtering capacity, we apply in this paper a mathematical modeling approach that extends the study of Apostu and Mackey (2012) by coupling their model to four different glucose-repression events and a simplified metabolic pathway. The model takes into account the major processes responsible for the determination of intracellular galactose dynamics: Gal3 and Gal1 activation, galactose transport through the Gal2 permease, phosphorylation by Gal1 kinase and dilution due to cell growth. The model reveals that bistability not only persists in the full GAL metabolic-gene network but is also dynamically robust (i.e., exhibited over a wide range of parameters), which means that it is adaptable to various conditions. The model is then examined to determine its sensitivity to different concentrations of the repressor (glucose) and its adaptability to a repressive oscillatory signal at different frequencies.

2. Mathematical modeling of the GAL regulon and the Leloir pathway

When discussing the cellular processes affected by galactose, we typically focus on two main branches, as shown in Fig. 1(A): (i) the metabolic branch, or the Leloir pathway that converts galactose into other forms suitable for energy consumption; and (ii) the genetic branch that consists of regulatory processes happening on a slower time scale. Galactose activates several feedback loops once transported into the cytosol. The other important sugar in yeast is raffinose, a trisaccharide composed of fructose, glucose and galactose. With respect to the galactose network, raffinose and glycerol neither activate, nor inhibit the galactose network, as galactose and glucose do, respectively. Hence, these sugars are often called non-inducible, non-repressible media (NINR) (Stockwell et al., 2015). In their presence, a basal level, or "leakage", in the expression of GAL80 and GAL3 mRNA is observed (with only 3–5 fold increase) (Giniger et al., 1985). Their overall effects on the galactose network are summarized in Table B1 of Appendix B).

In the following model development, proteins of the galactose network are denoted by small letters (e.g. Gal1p and Gal2p), whereas capital letters are used for genes (e.g. GAL3 and GAL2). GAL3, GAL80, GAL2 and GAL1 mRNA expression levels are denoted by M_3, M_{80}, M_2 and M_1, respectively, whereas their protein concentrations are denoted by G_3, G_{80}, G_2 and G_1, respectively. Throughout our analysis, we will assume that protein translation is directly proportional to the expression level of mRNA produced.

2.1. GAL regulon

The gene regulation part of our model combines assumptions from Apostu and Mackey (2012) with recent experimental results on the existence of a positive feedback loop mediated by Gal1p (Abramczyk et al., 2012; Venturelli et al., 2012). The kinetic reactions pertaining to the gene regulatory network are shown schematically in Fig. 1(B).

As indicated by panel B1 of Fig. 1, Gal4p dimers (G_{4d}) have a high affinity for regions of the GAL promoter known as upstream activating sequences ($[UAS]_g$), which are 17 base-pair sequences. Depending on the respective mRNA species, these sequences can occur more than once. It has been shown experimentally that for the GAL3 and GAL80 genes, there is a single $[UAS]_g$, while for the

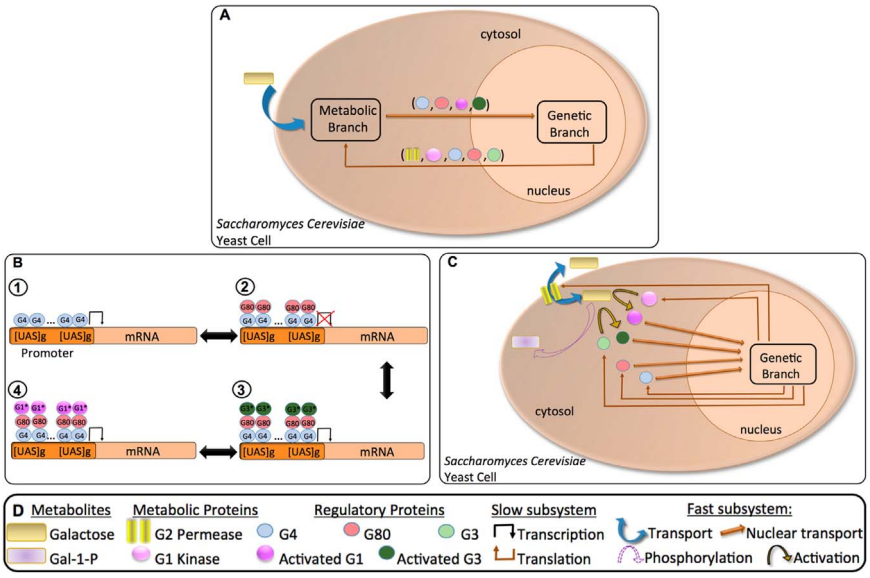

Fig. 1. (A) Schematic illustration of the full galactose network, containing its genetic and metabolic branches. (B) Schematic illustration of the GAL regulon and the effects of the proteins on their own transcription: (1) Gal4p dimers ($[G_4\colon G_4]$) bind to the upstream activating sequence ($[UAS]_g$). (2) In the absence of galactose, Gal80p dimers ($[G_{80}\colon G_{80}]$) bind to Gal4p dimers. (3) In the presence of galactose, activated Gal3 proteins (G_3^*) bind to $[G_4\colon G_4]\colon [G_{80}\colon G_{80}]$ complex, inducing network activation. (4) Gal1p dimers ($[G_1^*\colon G_1^*]$) replace Gal3p dimers ($[G_3^*\colon G_3^*]$) in the complex. The repeated dots (⋯) in each subpanel represent the series of binding reactions undertaken by each mRNA species considered. (C) Schematic illustration of the metabolic branch (to be read from top-left corner) showing how via facilitated diffusion, galactose gets transported across the plasma membrane by the permease Gal2p (G_2). (D) Table showing the definition of symbols used in previous panels.

other GAL mRNAs, there are up to 5 sequences (Ideker et al., 2001; Sellick et al., 2008; de Atauri et al., 2004). The $G_{4d}\colon [UAS]_g$ complex has a high affinity to the Gal80 dimer (G_{80d}) when raffinose is present (panel B2). This dimer acts as an inhibitor and therefore creates a negative feedback on its own transcription. In the presence of galactose, transcription is induced via activated Gal3p dimers ($[G_3^\star\colon G_3^\star]$), which remove the inhibition exerted by Gal80p dimers (panel B3) by generating the tripartite complex $[G_{4d}\colon G_{80d}\colon G_{3d}]$ in high proportion in the nucleus during the first 10 min of galactose induction (Abramczyk et al., 2012). This is then followed by the substitution of Gal3p by Gal1p dimers to form the new tripartite complex $[G_{4d}\colon G_{80d}\colon G_{1d}]$ (panel B4) for more efficient transcription.

Based on the above discussion, we conclude that the model should contain the following two reactions: the interactions of Gal3p (G_3) and Gal1p (G_1) with intracellular galactose (G_i) as determined by the two transitions

$$G_3 \xrightarrow{F_3(G_i)} G_3^*, \quad G_1 \xrightarrow{F_1(G_i)} G_1^*, \tag{1}$$

where F_3 and F_1 are the reaction rates appearing in Table B1, and G_3^* and G_1^* are the active forms of G_3 and G_1, respectively. The exact activation mechanism of these reactions has not been elucidated so far. Therefore, we assume here that they follow a saturating function with Michaelis–Menten kinetics

$$F_k = \frac{\kappa_{C,k} G_i}{K_S + G_i}, \quad k \in \{1, 3\}, \tag{2}$$

where $\kappa_{C,1}$ and $\kappa_{C,3}$ are the maximal catalytic rates and K_S is the galactose concentration for half-maximal activation. For simplicity, we will assume that intracellular galactose binds with the same half-maximal activation to both G_3 and G_1 proteins.

There are several promoter conformations that play a crucial role in determining the probability of gene expression. In our model, we will use ($\mathcal{R}$) to describe the probability of transcription, also known as the fractional transcription level, which is similar to that used in Apostu and Mackey (2012) and Venkatesh et al. (1999). It represents the fraction of the GAL promoters that is active and is expressed by

$$\begin{aligned}\mathcal{R}_1(G_{80}, G_3^*, G_1^*) &= 1 - \frac{D_2}{D_1 + D_2 + D_3 + D_4} \\ &= 1 - \frac{1}{1 + \dfrac{K_{D,80}K_{B,80}}{G_{80}^2} + \dfrac{(G_3^*)^2}{K_{D,3}K_{B,3}} + \dfrac{(G_1^*)^2}{K_{D,1}K_{B,1}K_{B,3}}},\end{aligned}$$

whenever the promoter contains one single $[UAS]_g$. D_1, D_2, D_3 and D_4 are the four promoter conformations, as described in Fig. 1 (B) and Table B1, and $K_{D,i}$ and $K_{B,i}$ (with $i \in \{1, 3, 80\}$) are the dissociation constants obtained using quasi-steady state (QSS) assumptions on the dimerization and on the binding reactions. A complete derivation of $\mathcal{R}_1$ is provided in Appendix B.

When the promoter, however, contains multiple $[UAS]_g$, the expression for the fractional transcription level becomes

$$\mathcal{R}_n(G_{80}, G_3^*, G_1^*) = 1 - \frac{1}{1 + \sum_{k=1}^{n}\left(\dfrac{\sqrt{K_{D,80}K_{B,80}}}{G_{80}}\right)^{2k} + \sum_{k=1}^{n}\left(\dfrac{G_3^*}{\sqrt{K_{D,3}K_{B,3}}}\right)^{2k} + \sum_{k=1}^{n}\left(\dfrac{G_1^*}{\sqrt{K_{D,1}K_{B,1}K_{B,3}}}\right)^{2k}}, \tag{3}$$

where n is the total number of $[UAS]_g$, a quantity that is equivalent to the number of G_4 dimers binding at the GAL promoter site, as

shown in Fig. 1(B). We assume that the promoter regions act independently of one another, i.e., G_4 dimers binding at one $[UAS]_g$ site would not affect subsequent binding reactions.

Assuming that the rates of change for the active proteins Gal3 and Gal1 are at QSS (see Eq. (B.1a)), we can write the fractional transcription level in Eq. (3) in terms of the inactivate proteins Gal3 and Gal1 as follows:

$$\mathcal{R}_n(G_{80}, G_3, G_1, G_i) = 1 - \frac{1}{1 + \sum_{k=1}^{n}\left(\frac{K_{80}}{G_{80}}\right)^{2k} + \sum_{k=1}^{n}\left(\frac{G_3 G_i}{K_3(K_S + G_i)}\right)^{2k} + \sum_{k=1}^{n}\left(\frac{G_1 G_i}{K_1(K_S + G_i)}\right)^{2k}}, \tag{4}$$

where the constants K_{80}, K_3 and K_1 are given by

$$K_{80} = \sqrt{K_{D,80}K_{B,80}},\ K_3 = \frac{\sqrt{K_{D,3}K_{B,3}}(\gamma_{G,3} + \mu)}{\kappa_{C,3}},$$
$$K_1 = \frac{\sqrt{K_{D,1}K_{B,3}K_{B,1}}(\gamma_{G,1} + \mu)}{\kappa_{C,1}}. \tag{5}$$

In the previous equations, $\gamma_{G,3}$ and $\gamma_{G,1}$ are the degradation rates of the proteins Gal3 and Gal1, respectively. We assume that the activation of these molecules does not effect the degradation process, and these parameters will also appear in the rates of change for the non-activated Gal3 and Gal1. Moreover, μ is another degradation rate, occurring due to cellular growth, which we will use hereafter to represent the dilution rate of all molecular species.

As in the previous regulon model of Apostu and Mackey (2012), we do not include Gal4p in our modeling approach, since GAL4 transcription is neither repressed by glucose (Timson, 2007), nor subject to the bistability property of the other Gal proteins (Acar et al., 2005). This, as a result, leaves us with three important regulatory proteins of the gene network; namely, Gal3p, Gal80p and Gal1p.

As mentioned previously, Gal3p creates a positive feedback loop within the system. By letting M_3 denote the level of GAL3 mRNA, we can express its galactose-driven transcription in terms of $\mathcal{R}_1$, with a maximal transcription rate $\kappa_{tr,3}$. We assume that GAL3 mRNA level is subject to cellular degradation at a rate γ_M and dilution at a rate μ. Based on this, we have

$$\frac{dM_3}{dt} = \kappa_{tr,3}\mathcal{R}_1(G_{80}, G_3, G_1, G_i) - (\gamma_M + \mu)M_3. \tag{6}$$

As described by Abramczyk et al. (2012), Gal3p is a "ligand sensor"; upon activation, it binds to galactose molecules and subsequently removes the transcriptional inhibition exerted by Gal80p. Its mRNA promoter region is characterized by having a single binding site for the Gal4p dimer. Dynamically, GAL3 mRNA is translated at a rate $\kappa_{tl,3}$ and the associated protein (G_3) is degraded at a rate $\gamma_{G,3}$. We also use the conversion factor c to account for the change in units (from mRNA copies to mM of proteins). A fraction of the Gal3p concentration is also activated by intracellular galactose (G_i), as described by Eq. (2). Thus,

$$\frac{dG_3}{dt} = \frac{\kappa_{tl,3}}{c}M_3 - \left(\gamma_{G,3} + \mu + \frac{\kappa_{C,3}G_i}{K_S + G_i}\right)G_3. \tag{7}$$

Gal80p is the inhibitory component of the GAL gene network. In the model, M_{80} represents GAL80 mRNA levels and $\kappa_{tr,80}$ and γ_M denote its transcription and degradation rates, respectively. Based on this, we conclude that

$$\frac{dM_{80}}{dt} = \kappa_{tr,80}\mathcal{R}_1(G_{80}, G_3, G_1, G_i) - (\gamma_M + \mu)M_{80}. \tag{8}$$

For the dynamic changes of the Gal80 protein, similar processes as those appearing in Eq. (7) for the Gal3 protein are considered, except for the activation induced by galactose binding, which is absent here. Denoting GAL80 translation rate by $\kappa_{tl,80}$ and Gal80p degradation rate by $\gamma_{G,80}$, we obtain

$$\frac{dG_{80}}{dt} = \frac{\kappa_{tl,80}}{c}M_{80} - (\gamma_{G,80} + \mu)G_{80}. \tag{9}$$

The presence of four $[UAS]_g$ on the GAL1 promoter region implies that its transcription must depend on $\mathcal{R}_4$. By letting $\kappa_{tr,1}$ and γ_M denote GAL1 transcription and mRNA degradation rates, respectively, the resulting equation governing M_1 dynamics becomes

$$\frac{dM_1}{dt} = \kappa_{tr,1}\mathcal{R}_4(G_{80}, G_3, G_1, G_i) - (\gamma_M + \mu)M_1. \tag{10}$$

To describe the dynamic changes in Gal1p concentration, we will use $\kappa_{tl,1}$ and $\gamma_{G,1}$ to denote GAL1 translation and Gal1p degradation rates, and use Michaelis–Menten kinetics of Eq. (2) to describe its activation by G_i. Based on this, the rate of change of Gal1p is

$$\frac{dG_1}{dt} = \frac{\kappa_{tl,1}}{c}M_1 - \left(\gamma_{G,1} + \mu + \frac{\kappa_{C,1}G_i}{K_S + G_i}\right)G_1. \tag{11}$$

From a metabolic point of view, G_1 kinase converts ATP and galactose into ADP and Gal1P, denoted by G_p. Gal1P is known to inhibit the kinase, through a mixed inhibition reaction involving the Gal1P product binding to the G_1 enzyme (Timson and Reece, 2002). This process is included in the metabolic reactions described in the following section.

2.2. Metabolic network

In our model, we will include the following reaction steps of the Leloir pathway (see Fig. 1(C)):

$$G_e \xleftrightarrow{G_2(\alpha)} G_i \xrightarrow{G_1(\kappa_{GK})} G_p \xrightarrow{\text{Metabolism}(\delta)} \text{Glycolysis},$$

where G_e and G_i are the extracellular and intracellular galactose concentrations. The symbols above the arrows represent the reactions of the Leloir pathway, with the specific enzymes involved (G_2 and G_1) as well as the reactions rates (shown between parentheses) for galactose transport (α), its phosphorylation (κ_{GK}) and G_p consumption (δ). Since G_i is known to be a transcriptional activator of the Leloir enzymes downstream from G_p, it is reasonable to assume that, overall, δ represents these processes in the form of a negative feedback loop. As a result, G_p is the last metabolite that we consider in our model.

Gal2p is a transmembrane, symmetric diffusion carrier and the main galactose transporter. GAL2 mRNA has two $[UAS]_g$ for activation, implying that its probability of expression can be described by $\mathcal{R}_2$, with a maximum transcription rate $\kappa_{tr,2}$. The rates of change for the GAL2 and Gal2p species are

$$\frac{dM_2}{dt} = \kappa_{tr,2}\mathcal{R}_2(G_{80}, G_3, G_1, G_i) - (\gamma_M + \mu)M_2 \tag{12a}$$

$$\frac{dG_2}{dt} = \frac{\kappa_{tl,2}}{c}M_2 - (\gamma_{G,2} + \mu)G_2, \tag{12b}$$

where γ_M and $\gamma_{G,2}$ are the degradation rates for GAL2 mRNA and Gal2p, respectively, and $\kappa_{tl,2}$ is the translation rate.

For the dynamics of the GAL1 mRNA and its associated protein, the last elements of the metabolic network, they have already been discussed in the regulatory network of (Eqs. (10) and 11).

Recall that galactose is transported via Gal2p by facilitated diffusion, with a maximal rate α and half-maximum transport K. We use the conversion factor c_g to convert the units from weight/volume ([% w/v]) to millimolars ([mM]). The transport of the molecule (T) across the plasma membrane is completely governed by the balance between extracellular and intracellular concentrations, as follows:

$$T(G_2, G_i) = \alpha G_2\left(\frac{c_g G_e}{K + c_g G_e} - \frac{G_i}{K + G_i}\right). \tag{13}$$

This expression stems from a simplification of a carrier-facilitated diffusion (Ebel, 1985) and is equivalent to the one found in de Atauri et al. (2005).

Inside the cell, galactose is converted to the phosphorylated form G_p via the Gal1p kinase. The phosphorylation is inhibited by the G_p product through a mixed inhibition (Timson and Reece, 2002; Rogers et al., 1970), and is described by a Michaelis–Menten function, having a maximum rate σ and a half-maximum activation κ_p, both dependent on the intracellular galactose concentration, as follows:

$$\sigma(G_i) = \frac{\kappa_{GK}K_{IU}K_{IC}}{K_{IU}K_m + K_{IC}G_i} = \kappa_{GK}X \tag{14a}$$

$$k_p(G_i) = \frac{(K_m + G_i)K_{IU}K_{IC}}{K_{IU}K_m + K_{IC}G_i} = (K_m + G_i)X, \tag{14b}$$

where $X = \frac{K_{IU}K_{IC}}{K_{IU}K_m + K_{IC}G_i}$. Galactose also activates Gal3 and Gal1 proteins. Hence, by considering galactose transport, its phosphorylation, its activation of Gal1p and Gal3p, as well as its dilution (μ), we can express the rate of change of this monosaccharide by the equation

$$\frac{dG_i}{dt} = T(G_2, G_i) - \frac{\sigma(G_i)}{\kappa_p(G_i) + G_p}G_1G_i - G_i\left(\frac{\kappa_{C,3}G_3}{K_S + G_i} + \frac{\kappa_{C,1}G_1}{K_S + G_i} + \mu\right), \tag{15}$$

where $T(G_2, G_i)$, $\sigma(G_i)$ and $k_p(G_i)$ are given by (Eqs. (13) and 14a and b), respectively.

The next metabolite in the Leloir pathway is G_p. Since none of the compounds downstream of Gal1p in the metabolic pathway has a feedback on the regulatory processes, the remaining metabolic reactions have been approximated by a single consumption parameter δ, as follows:

$$\frac{dG_p}{dt} = \frac{\sigma(G_i)}{\kappa_p(G_i) + G_p}G_1G_i - (\delta + \mu)G_p. \tag{16}$$

2.3. Galactose network model under glucose repression

Given that glucose is a repressor of the galactose network, we will examine how cells respond to an oscillatory glucose signal in the presence of galactose. Based on experimental evidence, there are four independent pathways by which glucose can repress the network.

2.3.1. Cellular growth

As mentioned previously, glucose is the energy source preferred by organisms, since they grow faster on glucose rather than on galactose, phenomenon which is reflected in our model in the dilution rate, μ. Thus, we use an increasing Hill function to express its dependency on glucose

$$\mu(R) = \mu_a + \frac{\mu_b R^{n_\mu}}{\mu_c^{n_\mu} + R^{n_\mu}}, \quad n_\mu > 0, \tag{17}$$

where R is the glucose concentration, $\mu_a + \mu_b$ is the maximum dilution rate, μ_c is the half-maximum dilution and n_μ is the Hill coefficient.

2.3.2. Transporter degradation

Experimental data indicates that glucose enhances vesicle degradation of the Gal2p transporter (Horak and Wolf, 1997; Ramos et al., 1989). To capture this effect, we assume here that the degradation rate of Gal2p (denoted by $\gamma(R)$ hereafter) follows a Hill function in its dependence on external glucose concentration

$$\gamma(R) = \gamma_{G,2} + \frac{\gamma_b R^{n_\gamma}}{\gamma_c^{n_\gamma} + R^{n_\gamma}}, \quad n_\gamma > 0, \tag{18}$$

where γ_c is the maximum degradation rate, γ_c is the half-maximum degradation and n_γ is the Hill coefficient.

2.3.3. Transcriptional regulation

Although the molecules involved in transcription have been discovered, most of the research in this area focused on presenting the overall reaction and the main factors without providing the necessary data for the quantification of the repression induced by glucose. Therefore, we approximate this process by

$$x(R) = \frac{1}{\left(\frac{R}{x_C}\right)^{n_x} + 1}, \quad n_x \geq 1, \tag{19}$$

where x_C is the half-maximum of this repressive process and n_x is the Hill coefficient. As suggested by Bhat (2008), the inhibitor molecule Gal80p is not affected by this repression mechanism.

2.3.4. Transporter competition

Gal2p is the main transporter of galactose and is a high-affinity transporter for glucose (Maier et al., 2002; Reifenberger et al., 1997), which means that both monosaccharides compete for the same transporter. To incorporate this competition, we assume that the rate of galactose transport depends on a scaling factor $y(R)$, given by

$$y(R) = (1 - y_b) + y_b\frac{y_c^{n_y}}{y_c^{n_y} + R^{n_y}}, \quad n_y > 0, \tag{20}$$

where y_c is the half-maximum transport repression by glucose.

2.4. Complete mathematical model of the galactose network in the presence of glucose

2.4.1. Nine dimensional (9D) GAL model

In the galactose network, metabolic reactions occur on a faster time scale than the rates of change of the proteins (Reznik et al., 2013). For example, transcription and translation occur with a time scale on the order of minutes, whereas transport via facilitated diffusion and phosphorylation occur at a rate greater than 500

times per minute (de Atauri et al., 2005). This implies that we can use a QSS approximation on Eq. (16) depicting the dynamics of the phosphorylated form of galactose (G_p). By solving for the equilibrium concentration of this compound ($G_{p,(ss)}$) (as shown in Appendix B), we can then replace G_p in Eq. (15) by its steady state. This produces a nine dimensional model (9D) for the galactose network, given by

$$\frac{dM_3}{dt} = \kappa_{tr,3}\chi(R)\mathcal{R}_1(G_{80}, G_3, G_1, G_i) - (\gamma_M + \mu(R))M_3 \tag{21a}$$

$$\frac{dM_{80}}{dt} = \kappa_{tr,80}\chi(R)\mathcal{R}_1(G_{80}, G_3, G_1, G_i) - (\gamma_M + \mu(R))M_{80} \tag{21b}$$

$$\frac{dM_2}{dt} = \kappa_{tr,2}\chi(R)\mathcal{R}_2(G_{80}, G_3, G_1, G_i) - (\gamma_M + \mu(R))M_2 \tag{21c}$$

$$\frac{dM_1}{dt} = \kappa_{tr,1}\chi(R)\mathcal{R}_4(G_{80}, G_3, G_1, G_i) - (\gamma_M + \mu(R))M_1 \tag{21d}$$

$$\frac{dG_3}{dt} = \frac{\kappa_{tl,3}}{c}M_3 - \left(\gamma_{G,3} + \mu(R) + \frac{\kappa_{C,3}G_i}{K_S + G_i}\right)G_3 \tag{21e}$$

$$\frac{dG_{80}}{dt} = \frac{\kappa_{tl,80}}{c}M_{80} - \left(\gamma_{G,80} + \mu(R)\right)G_{80} \tag{21f}$$

$$\frac{dG_2}{dt} = \frac{\kappa_{tl,2}}{c}M_2 - \left(\gamma(R) + \mu(R)\right)G_2 \tag{21g}$$

$$\frac{dG_1}{dt} = \frac{\kappa_{tl,1}}{c}M_1 - \left(\gamma_{G,1} + \mu(R) + \frac{\kappa_{C,1}G_i}{K_S + G_i}\right)G_1 \tag{21h}$$

$$\frac{dG_i}{dt} = \alpha y(R)G_2\left(\frac{c_g G_e}{K + c_g G_e} - \frac{G_i}{K + G_i}\right) - \frac{2\sigma(G_i)G_iG_1}{k_p(G_i) + \sqrt{k_p(G_i)^2 + \frac{4\sigma(G_i)G_iG_1}{\delta}}} - G_i\left(\frac{\kappa_{C,3}G_3}{K_S + G_i} + \frac{\kappa_{C,1}G_1}{K_S + G_i}\right) - \mu(R)G_i, \tag{21i}$$

where $\mathcal{R}_n(G_{80}, G_3, G_1, G_i)$ is defined in Eq. (3) and the functions $\sigma(G_i)$ and $k_p(G_i)$ in Eqs. (14a–b). Notice that, in the absence of glucose, we have, according to (Eqs. (17)–20), $\chi(R) = y(R) = 1$, $\gamma(R) = \gamma_{G,2}$ and $\mu(R) = \mu_a$.

2.4.2. Five dimensional (5D) GAL model

The 9D model can be further reduced to a five dimensional (5D) model by applying QSS approximation to the variables representing the various mRNA species of Eqs. (21a–d), based on the fact that their degradation rates are one order of magnitude larger than those of their corresponding proteins. This 5D model is given by

$$\frac{dG_3}{dt} = \frac{\kappa_{tl,3}\kappa_{tr,3}\chi(R)}{c\left(\gamma_M + \mu(R)\right)}\mathcal{R}_1(G_{80}, G_3, G_1, G_i) - \left(\gamma_{G,3} + \mu(R) + \frac{\kappa_{C,3}G_i}{K_S + G_i}\right)G_3 \tag{22a}$$

$$\frac{dG_{80}}{dt} = \frac{\kappa_{tl,80}\kappa_{tr,80}}{c\left(\gamma_M + \mu(R)\right)}\mathcal{R}_1(G_{80}, G_3, G_1, G_i) - \left(\gamma_{G,80} + \mu(R)\right)G_{80} \tag{22b}$$

$$\frac{dG_2}{dt} = \frac{\kappa_{tl,2}\kappa_{tr,2}\chi(R)}{c\left(\gamma_M + \mu(R)\right)}\mathcal{R}_2(G_{80}, G_3, G_1, G_i) - \left(\gamma(R) + \mu(R)\right)G_2 \tag{22c}$$

$$\frac{dG_1}{dt} = \frac{\kappa_{tl,1}\kappa_{tr,1}\chi(R)}{c\left(\gamma_M + \mu(R)\right)}\mathcal{R}_4(G_{80}, G_3, G_1, G_i) - \left(\gamma_{G,1} + \mu(R) + \frac{\kappa_{C,1}G_i}{K_S + G_i}\right)G_1 \tag{22d}$$

$$\frac{dG_i}{dt} = \alpha y(R)G_2\left(\frac{G_e}{K + G_e} - \frac{G_i}{K + G_i}\right) - \frac{2\sigma(G_i)G_iG_1}{k_p(G_i) + \sqrt{k_p(G_i)^2 + \frac{4\sigma(G_i)G_iG_1}{\delta}}} - G_i\left(\frac{\kappa_{C,3}G_3}{K_S + G_i} + \frac{\kappa_{C,1}G_1}{K_S + G_i}\right) - \mu(R)G_i. \tag{22e}$$

As before, the functions $\mathcal{R}_n(G_{80}, G_3, G_1, G_i)$, $\sigma(G_i)$, $k_p(G_i)$, $\mu(R)$, $\gamma_2(R)$, $\chi(R)$ and $y(R)$ are defined by Eqs. (3), (14a), (14b), (17), (18), (19) and (20), respectively. It was previously mentioned that glucose (R) induces repression of the GAL network. In its absence (i.e., when $R = 0$), the model will be called hereafter "reduced 5D model", whereas in the presence of glucose-repression, it will be called the "extended 5D model".

All model variations of the GAL network presented above have been implemented in XPPAUT and MATLAB, for further analysis and numerical simulations. Readers can refer to Appendix A for more information on the software techniques employed.

2.5. Model parameters

Parameter values of the models listed above have been mostly estimated using experimental data obtained from the same yeast strain under similar laboratory conditions.

2.5.1. Galactose parameters

The rates contained in Table 1 are: (a) transcription and translation rates for all the four GAL mRNAs; (b) degradation and dilution rates for all intracellular species; (c) dissociation constants of compounds involved in the genetic regulation, and (d) metabolic rates including transport and phosphorylation. Whenever possible, these values are chosen to fit experimental and/or literature data. Calculations and detailed derivations of these results can be found in the following subsection. As for the parameters involved in galactose-induced activation, they are estimated using numerical simulations under the assumption that the dynamics of the model must exhibit bistability. Parameter values listed in Table 1 are representative of a wild-type cell.

2.5.2. Glucose parameters

The parameters used in modeling repression are obtained by fitting the mathematical expression of these repressive processes to experimental data using the "Cftool" toolbox and the Genetic Algorithm (see Table 2). These data fitting techniques were presented in Appendix A. Since glucose administered in experiments is usually expressed in units of [% w/v], the fitted parameters representing half-maximum activations have the same units. The Hill coefficients n_μ and n_γ are set to 1, to provide an ideal Michaelis–Menten relation representing the effect of glucose on

Table 1
Values of the model parameters of the galactose network. References are provided when the exact values of these parameters have been measured or estimated from experimental data.

Symbol	Model value	Definition [units]	References
κ_{r3}	0.329	M_3 transcription rate $\left[\frac{\text{copies}}{\text{cell}\times\text{min}}\right]$	Estimated (see Appendix A)
κ_{r80}	0.147	M_{80} transcription rate $\left[\frac{\text{copies}}{\text{cell}\times\text{min}}\right]$	
κ_{r2}	0.678	M_2 transcription rate $\left[\frac{\text{copies}}{\text{cell}\times\text{min}}\right]$	
κ_{r1}	1.042	M_1 transcription rate $\left[\frac{\text{copies}}{\text{cell}\times\text{min}}\right]$	
κ_{l3}	645	G_3 translation rate $\left[\frac{\text{molecules}}{\text{copies}\times\text{min}}\right]$	Estimated (see Appendix A)
κ_{l80}	210	G_{80} translation rate $\left[\frac{\text{molecules}}{\text{copies}\times\text{min}}\right]$	
κ_{l2}	800	G_2 translation rate $\left[\frac{\text{molecules}}{\text{copies}\times\text{min}}\right]$	
κ_{l1}	187	G_1 translation rate $\left[\frac{\text{molecules}}{\text{copies}\times\text{min}}\right]$	
c	4.215×10^{7}	Conversion factor $\left[\frac{\text{molecules}}{\text{cell}\times\text{mM}}\right]$	Estimated (see Appendix A)
c_g	55.38	Conversion factor for G_e $\left[\frac{\text{mM}}{\%\,\text{w/v}}\right]$	Estimated (see Appendix A)
μ_a	4.438×10^{-3}	Dilution rate [min^{-1}]	Tyson et al. (1979)
γ_M	4.332×10^{-2}	M_3 degradation rate [min^{-1}]	Holstege et al. (1998), Bennett et al. (2008)
$\gamma_{G,3}$	7.112×10^{-3}	G_3 degradation rate [min^{-1}]	Ramsey et al. (2006)
$\gamma_{G,80}$	2.493×10^{-3}	G_{80} degradation rate [min^{-1}]	
$\gamma_{G,2}$	0	G_2 degradation rate [min^{-1}]	
$\gamma_{G,1}$	0	G_1 degradation rate [min^{-1}]	
$K_{D,80}$	3×10^{-7}	$G80_d$ dissociation constant [mM]	Melcher and Xu (2001)
$K_{B,80}$	5×10^{-6}	D_2 dissociation constant [mM]	Lohr et al. (1995)
$K_{B,3}$	6×10^{-8}	D_3 dissociation constant [mM]	Acar et al. (2005)
$K_{B,1}$	6×10^{-8}	D_4 dissociation constant [mM]	Bistability[a]
$K_{D,3}$	1.25×10^{-2}	$G3^*_d$ dissociation constant [mM]	
$K_{D,1}$	1	$G1^*_d$ dissociation constant [mM]	
K_S	4000	G_3 and G_1 half-maximum activation [mM]	
$\kappa_{C,3}$	0.5	G_3 activation rate $\left[\frac{1}{\text{mM}\times\text{min}}\right]$	Bistability[a]
$\kappa_{C,1}$	8×10^{-5}	G_1 activation rate $\left[\frac{1}{\text{mM}\times\text{min}}\right]$	
α	4350	Maximum rate of symmetric facilitated diffusion [min^{-1}]	de Atauri et al. (2005)
κ_{GK}	702	Experimentally measured phosphorylation rate of G_i [min^{-1}]	van den Brink et al. (2009)
δ	59,200	Rate of Gal1p metabolism [min^{-1}]	de Atauri et al. (2005)
K	1	Half-maximum concentration for the transport process [mM]	de Atauri et al. (2005)
K_m	1.2	Half-maximum concentration for phosphorylation [mM]	Timson and Reece (2002)
K_{IC}	160	Competitive inhibition constant [mM]	Timson and Reece (2002)
K_{IU}	19.1	Uncompetitive inhibition constant [mM]	Timson and Reece (2002)

[a] Determined based on guaranteed existence of bistability.

cellular growth and degradation of the Gal2p transporter. The parameters describing these two processes were estimated using "Cftool" (see Table A1). The other two glucose-induced repressive processes (i.e., transcriptional repression and transporter competition), require more complex fitting procedures. The Hill coefficients n_x and n_y are chosen to be 1, because it minimizes the error produced by the Genetic Algorithm (see Table A2).

Table 2
Kinetic parameters of glucose repression in the extended 5D model. Half-maximum activations are in units of weight/volume ([% w/v]). "Cftool" was used to fit the functions describing dilution and G_2 transporter degradation, whereas the Genetic Algorithm was used to fit the parameters involved in the last two processes of glucose repression.

Symbol	Model value	Definition [units]
μ_b	0.00512	Dilution rate in glucose [min^{-1}]
μ_c	0.3611	Half-maximum activation for dilution [% w/v]
n_μ	1	Hill coefficient for dilution [unitless]
γ_b	0.001416	Gal2p degradation rate [min^{-1}]
γ_c	0.8592	Half-maximum activation for degradation [% w/v]
n_γ	1	Hill coefficient for Gal2p degradation [unitless]
x_c	0.2443	Half-maximum activation for transcriptional regulation [% w/v]
n_x	1	Hill coefficient for transcriptional regulation [unitless]
y_b	0.0003	Increase in the competition rate due to repression [min^{-1}]
y_c	2.9989	Half-maximum activation for repressive competition [% w/v]
n_y	1	Hill coefficient for the competition between glucose and galactose for the Gal2p transporter [unitless]

3. Results

Given the complexity of the 9D model, we first focus on the dynamics of the reduced and extended 5D models. We begin by examining how the bifurcation structure of these models is altered in response to biological changes. By doing so, we can draw close connections between predicted model behaviours and observed experimental results. We will then examine the temporal response of the extended 5D model to periodic forcing by extracellular glucose to elucidate the low-pass filtering nature of the GAL network as suggested by Bennett et al. (2008).

3.1. Bistability with respect to galactose

3.1.1. Steady state behaviour of metabolic proteins

To examine how the model depends on extracellular galactose and glucose, we study the steady state behaviour of the (reduced and extended) 5D models. The 5D model described by Eqs. (22a–e) is used for this purpose, since the QSS approximation assumed for the mRNA level in this model will not alter its steady state properties.

To conduct this analysis, a physiological range for extracellular galactose G_e is specified. This can be done by using galactose induction curves obtained under various experimental conditions (such as the type of strain and growth conditions used). Given the extensive data available, we focus our analysis only on the wild type strain K699 and choose, as a result, the initial range of 0–0.08% w/v for G_e to plot the one-parameter bifurcation of various metabolites of the reduced 5D model with respect to G_e within this range.

Fig. 2 shows model outcomes of the equilibrium concentrations associated with the four main Gal proteins: G_3 (panel A), G_{80} (panel B), G_2 (panel C) and G_1 (panel D) with respect to G_e. In all cases, bistability is exhibited by the four variables in the form of two branches of attracting equilibria (solid lines), an upper branch that corresponds to the induced state and a lower branch that corresponds to the uninduced state. These branches overlap over a wide range of values for G_e, separated by a branch of unstable equilibria (dashed line), i.e., a branch of physiologically unattainable steady states. The right saddle node at the intersection of the

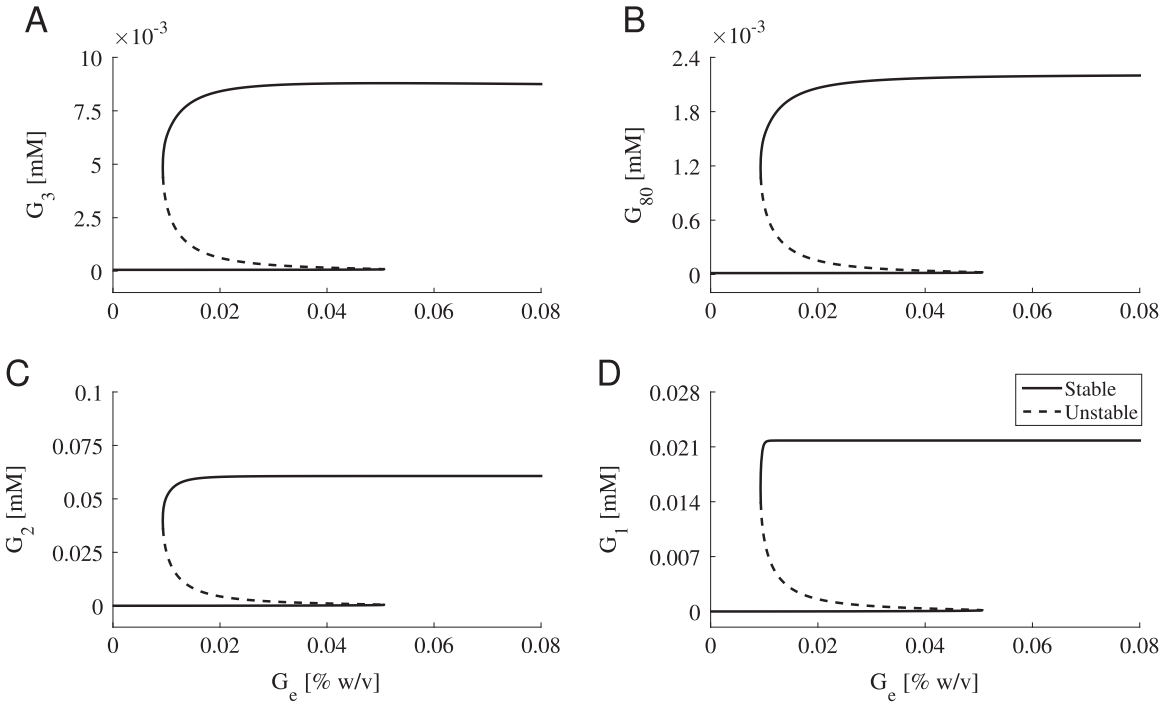

Fig. 2. One-parameter bifurcation of various proteins as a function of the extracellular galactose concentration (G_e), measured in units of [% w/v]. The four panels show the steady state values of (A) the regulatory protein Gal3 (G_3); (B) the inhibitory regulatory protein Gal80 (G_{80}); (C) the permease Gal2 (G_2); and (D) the regulatory and enzymatic protein Gal1 (G_1). Solid lines refer to the stable branches of attracting equilibria, whereas dashed lines represent the unstable branches of equilibria, separating the two stable branches within the bistable regime. This initial range of 0–0.8% w/v for G_e was chosen to make the bistability regime distinguishable between the bifurcation diagrams.

Table 3
Comparison between the fold difference calculated from induced versus uninduced states of the Gal proteins, from experimental and modelling results. The bimodality observed in the fluorescence histograms of different studies gives the calculated folds in the "Experimental values" column. "Model results" are the fold differences calculated from the upper and the lower branches of stable equilibria in the bistable switches of Fig. 2. Although it is not present in our 9D model, Gal10 protein (G_{10}) is shown here as a reference of the ratio induced-to-uninduced states for the metabolic GAL proteins.

Gal protein	Ratios of the induced-to-uninduced states	
	Experimental values	Model results
G_3	33–37.5,[a] 40–330[b]	65
G_{80}		100
G_2		144–4320
G_1		144–6852
G_{10}	30–100[c]	

[a] Acar et al. (2005).
[b] Acar et al. (2010).
[c] Venturelli et al. (2012).

unstable and stable branches of Fig. 2 has a numerical value of 0.05% w/v. It represents the concentration of G_e that produces full induction of the network, consistent with that of K699 yeast strain determined by Bennett et al. (2008).

Next, we compare the ratios of the induced-to-uninduced states of the Gal1 and Gal10 mRNA within the bistable regime to those observed experimentally (Acar et al., 2005, 2010; Venturelli et al., 2012). The apparent discrepancies (see Table 3) may be due to the experimental data used to estimate the transcriptional and translational rates in our reduced 5D model, which is not derived from the same yeast strain (see Appendix A for the detailed estimation). It could be also due to the stochastic nature of the data acquired using cultures that contained many cells, unlike our numerical results that are generated using deterministic single-cell models.

Overall, these results reveal that the bistability studied in Apostu and Mackey (2012) is not only conserved in our GAL network, but is also an inherent property of the GAL regulon rather than the metabolic subnetwork. The induced-to-uninduced ratios are in agreement with certain experimental studies (Acar et al., 2005, 2010; Venturelli et al., 2012) and show that this ratio is most sensitive to perturbations in the transcriptional and translational rates. The analysis of the steady state behaviour of G_i with respect to G_e is left for Appendix B.

3.1.2. *Two-parameter bifurcations as a measure of sensitivity*

To assess the sensitivity of the bistable regime to parameter perturbations that are representative of variations in yeast strains, we study here how the two saddle nodes of Figs. 2 and B1 of Appendix B are affected by changes in the other rates of the system and how they alter the range of the bistable regime. These changes could reflect yeast strain variability due to genetic mutations which can create different functional properties or different growth rates and can either hinder or induce reactions by varying external factors.

We begin first by considering the two-parameter bifurcations that uncover how transcriptional repression of the Gal proteins affects the bistability regime. Fig. 3(A)–(D) displays in grey (white) the regimes of bistability (monostability) enclosed by black lines that determine the location of the left and right limit points (or saddle nodes) of Fig. 2. The monostable (white) regimes could either correspond to the induced state (to the right of the grey regimes) or uninduced state (to the left of the grey regimes). As shown, a decrease in the transcriptional rates of Gal3 and Gal2 proteins, involved in positive feedbacks, can extend this regime (panels A and C, respectively) by shifting the right limit point further to the right. A major decrease in the transcription rate of Gal2, however, can eventually shift the system into the uninduced monostable regime, provided that G_e is small enough. The transcription rates of Gal80 and Gal1, on the other hand, act in an opposite fashion (panels B and D, respectively). These results suggest that different mutants can have different dynamic properties. This may explain why

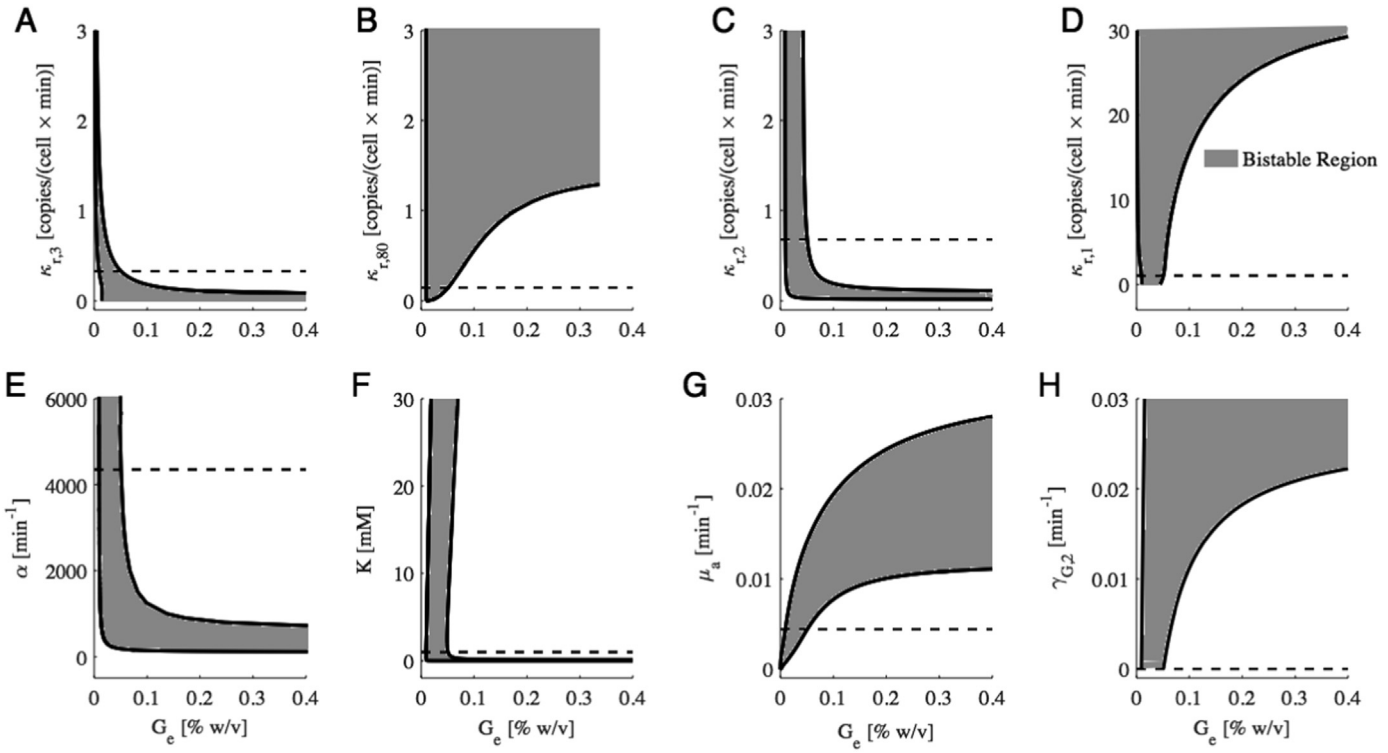

Fig. 3. Two-parameter bifurcations in the reduced 5D model with respect to extracellular galactose (G_e) and other kinetics parameters of the model. These include (A) Gal3 transcription rate ($\kappa_{r,3}$); (B) Gal80 transcription rate ($\kappa_{r,80}$); (C) Gal2 transcription rate ($\kappa_{r,2}$); (D) Gal1 transcription rate ($\kappa_{r,1}$); (E) Gal2-dependent galactose transport rate (α); (F) half-maximum transport (K); (G) dilution rate (μ), due to cellular growth; and (H) Gal2 degradation rate ($\gamma_{G,2}$). Each panel depicts the limit points (black lines), along with the bistable (grey) and the monostable (white) regimes. The dashed lines in these panels represent the default parameter values. Notice the presence of the cusp in panels A and B, the dependence of the left limit point on G_e in panel F, and the absence of the right limit point for high values of the parameter along the vertical axis, in panels B, D, G and H.

bistability was not observed by all research groups. Since yeast cultures are heterogenous, each cell culture can be described by a parameter set belonging to a particular stability regime of the two-parameter bifurcation.

We investigate the dynamics of the reduced 5D model in response to other parameter variations representing potential mutations, in Fig. 3(E)–(H). Our results in Fig. 3(E) reveal that when the rate of transport, α, is higher than its default value for wild type, little effect on bistability is observed. However, once the transport is impeded, the bistability regime broadens and the fully induced state may become unattainable (depending on initial conditions).

The bistability regime of the GAL network is also dependent on how rapidly yeast cells grow. Indeed, Fig. 3(G) shows that a lower growth rate (i.e. higher dilution rate μ_a than its default value) leads to a wider bistable regime. Similar results are observed in Fig. 3 (H) when increasing the degradation rate of the transporter. In this case, we see an increase in the bistability regime of the GAL system subsequent to a decrease in the capacity of the cells to be fully induced, which is equivalent to an increase in the effect of the inhibitory proteins.

In all of these cases discussed above, the two limit points of the two-parameter bifurcations (i.e., the boundaries of the bistable grey regimes) are present, with the left one mostly remaining stationary at one specific concentration of extracellular galactose G_e. The two-parameter bifurcation associated with the half-maximum transport K is the only one that does not follow the same pattern. Indeed, Fig. 3(F) shows that increasing K causes the left limit point to shift to the right, increasing the width of the monostable regime associated with the uninduced steady state. This could be beneficial for the cell as it may allow it to compensate for problems in the galactose induction, not only of yeast strains, but potentially of other eukaryotic cells as well.

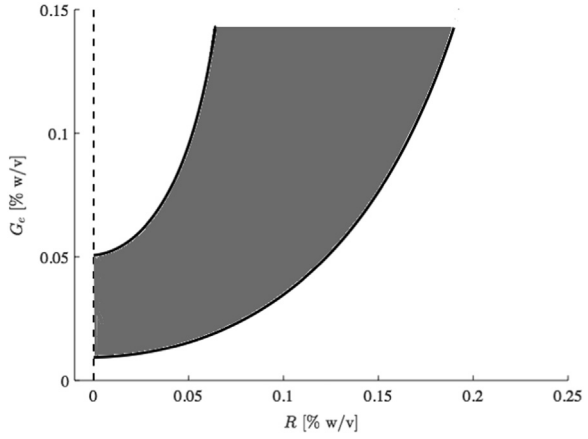

Fig. 4. Two parameter bifurcations with respect to extracellular galactose (G_e) and glucose (R), for a yeast strain which shows the bistable regime (in grey) bounded by the limit points as defined in (Fig. 3). The vertical dashed line represents the default parameter values of R.

The bistability regime with respect to the inducer (galactose) is also sensitive to the repressor (glucose). Fig. 4 portrays this sensitivity as a two-parameter bifurcation, with respect to G_e and glucose (R), which is qualitatively similar to the one seen in Venturelli et al. (2015) and to the landscape diagram of Stockwell et al. (2015). With the parameter combinations shown in Tables 1 and 2, we predict that the bistability property will persist even when no repressor (R) is present, a feature not mentioned in Venturelli et al. (2015). In an experimental setting, we expect the system to exhibit bistability (in the form of binary response) if the administered glucose concentration is less than 0.2% w/v and G_e is higher than 0.01% w/v.

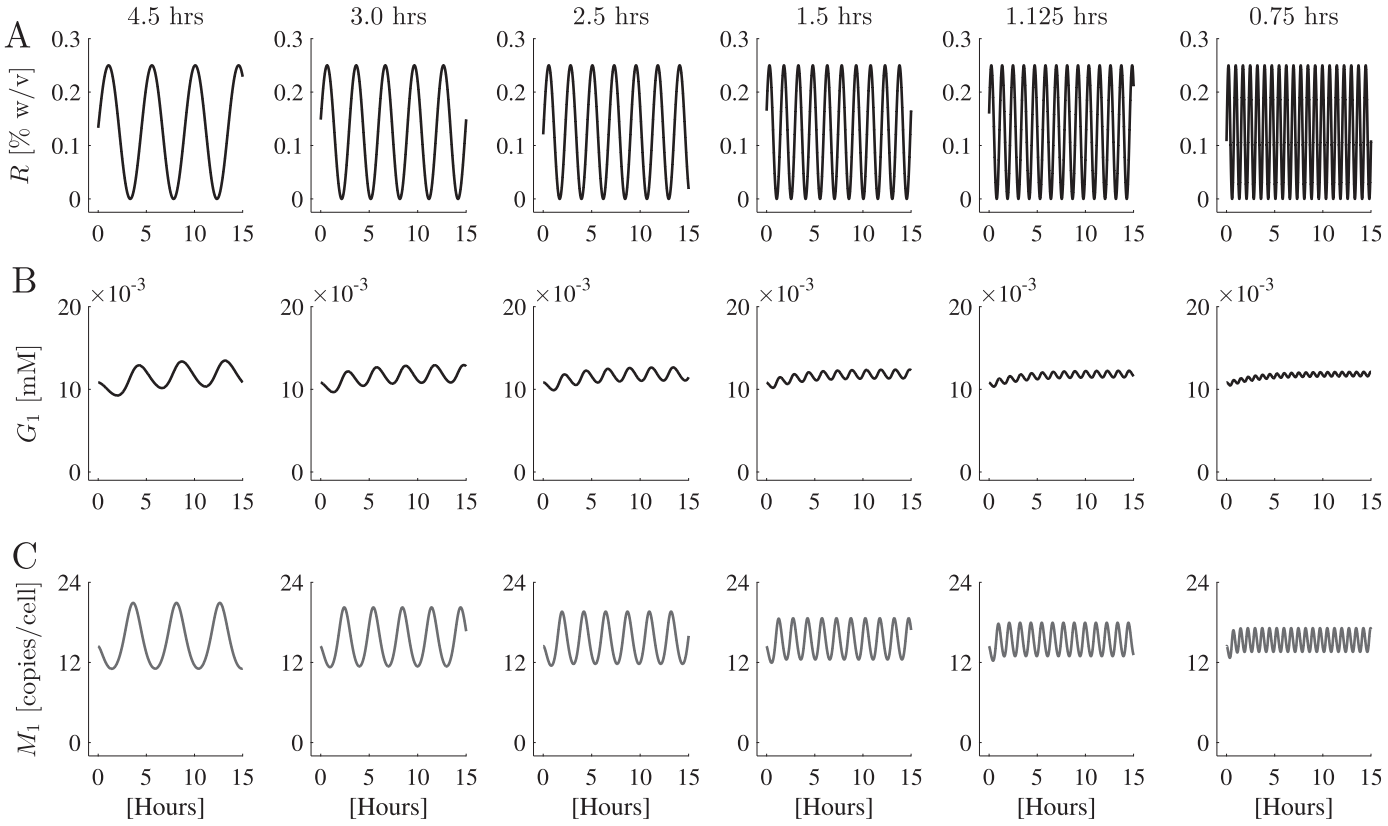

Fig. 5. Model response to oscillatory glucose input signal, generated using the 5D and 9D models for wild-type cells. (A) Extracellular glucose forcing with a period of 4.5, 3.0, 2.25, 1.5, 1.125 and 0.75 h is applied on the GAL network. (B) Gal1 output signal (G_1), generated from the extended 5D model, showing adaptation after a transient period of 5 h. (C) GAL1 mRNA output signal (M_1), generated from the 9D model, showing adaptation after only one hour.

3.2. Temporal response to an oscillatory glucose input

One important aspect of the GAL network established experimentally is its low-pass filtering capacity when wild-type and GAL2 mutant yeast cells, grown on a background medium of 0.2% w/v galactose, are subjected to a periodic glucose forcing of amplitude 0.125% w/v and a baseline of 0.125% w/v (Bennett et al., 2008), identical to that shown in Fig. 5(A). The two main features associated with this filtering capacity is the decline in the amplitude and phase of the output response (both determined experimentally by measuring GAL1 mRNA expression level). Here, we analyze this phenomenon using the extended 5D and 9D GAL models, to determine whether this behaviour is captured by both.

3.2.1. Dynamics of wild-type cells

Using the extended 5D model, the output of the GAL network for the wild-type strain (corresponding to the default parameter values) in response to glucose oscillations is shown in Fig. 5(B). As shown, the amplitude of the G_1 output signal decreases when the frequency of the glucose input signal increases. This behaviour is accompanied by a transient period of 5 h in which the output signal gradually ascents to an elevated baseline while oscillating. Our numerical results reveal that bistability and the phase of the glucose oscillatory input signal are the two key factors causing the elevation in the baseline, whereas the presence of various time scales within the model is responsible for creating the inverse correlation between the amplitude of output signal and the frequency of the input signal. Furthermore, akin to the experimental recordings of Bennett et al. (2008) showing the GAL1 mRNA output signal (upstream from G_1), our numerical results also display ascent in the baseline, but with a shorter transient of around 1 h. This suggests that although the reduced model possesses the core structure of the GAL network, the QSS assumptions may undermine the ability of the model to capture the proper length of the transient.

Due to the presence of discrepancy in the transients between experimental and numerical results (obtained from the extended 5D model), we turn our attention now to the 9D model to analyze the effects of QSS assumption on its response to oscillatory glucose input signal. We do so by plotting the GAL1 mRNA expression level as an output signal of the model when the oscillatory glucose input signal of Fig. 5(A) is applied. Fig. 5(C) shows that the inverse correlation between amplitude and frequency is preserved by the 9D model, and that the oscillations in the output signal exhibit higher peaks and more pronounced mRNA production during glucose decline in each cycle of the input signal. The figure also shows that the transient occurring before the oscillations in GAL1 mRNA reach a baseline lasts about 1 h, which is consistent with the value observed experimentally (Bennett et al., 2008). These results indicate that the 9D model is necessary when analyzing the temporal and transient dynamics of the system.

3.2.2. Modelling the GAL2Δ strain

As a test to validate the model against experimental data, we examine the predicted response of a GAL2 mutant strain (GAL2Δ) to periodic external glucose forcing. Bennett et al. (2008) described such a mutant as requiring ten times more galactose for full induction than the wild-type strain. To capture this effect in our simulations, the mutant is modelled by decreasing the transport rate α from 4350 to 702 min^{-1}. As demonstrated in Fig. 3(E), such small value of the parameter broadens the bistability regime of the galactose network, causing the right limit point to occur at higher G_i and making the monostable regime of the induced state less attainable.

Table 4
The four measures used to characterize the output signals of the 5D and 9D models.

Measures	Notation and definitions
Normalized mean	$\mathcal{M}_i = \frac{\bar{S}_i}{\max_{i=1\ldots N}(\bar{S}_i)}$, where $\bar{S}_i = \frac{1}{L}\int_0^L$ output dt, L=20 min and N=6 is the total number of input signals tested.
Normalized amplitude	$A_i = \frac{\left(\max_{[0,L]}(S_i) - \min_{[0,L]}(S_i)\right)/2}{\max_i\left\{\left(\max_{[0,L]}(S_i) - \min_{[0,L]}(S_i)\right)/2\right\}}$, where S_i is the output signal for all i = 1, …, 6.
Upstroke phase	U_i: The duration of the upstroke between a maximum and a preceding minimum averaged over the period T of the output signal S_i, i = 1, …, 6.
Phase shift	$\phi_i = \phi_{\text{input}_i} - \phi_{\text{output}_i}$: The difference between the phase of the input signal (ϕ_{input_i}) and the output signal (ϕ_{output_i}), i = 1, …, 6, as determined by the Hilbert transform defined in Appendix A.

As in the previous computational setting, the GAL2-mutant model is again subjected to a background medium of 0.2% w/v galactose and 0.125% w/v glucose for 24 h (to allow for the system to reach equilibrium), followed by the addition of an oscillatory glucose input signal of increasing frequencies. The responses of the mutant strain according to the 5D and 9D models are shown in Fig. B2 of Appendix B. Qualitatively, the output signals G_1 and M_1 for the 5D and 9D models, respectively, show an adaptation behaviour similar to the numerical results seen for the wild-type strain models of panels B and C in Fig. 5. At low frequencies, however, the mutant model shows no elevation in baseline, unlike the wild-type model.

3.2.3. *Quantification of model responses*

For a thorough understanding of the results presented in Figs. 5 and B.2, we use several measures to characterize the oscillatory output signal S_i (where i = 1, …, 6 is the total number of input signals of various frequencies, as shown in Fig. 5(A)) generated numerically at steady state when both the input and output signals are oscillating in tandem with each other. Four measures, defined in Table 4, have been used; these include the normalized mean ($\mathcal{M}_i$), the normalized amplitude (A_i) and the upstroke phase (U_i) of the signal as well as the phase difference, or phase shift (ϕ_i) between the phase of the input and output signals, as defined by the Hilbert transform. Given that Bennett et al. (2008) varied the frequency of the glucose input signal, we apply here a similar strategy, by calculating these measures across a whole range of frequencies.

The numerical results associated with these four measures are plotted in Fig. B3 of Appendix B, and explicitly listed in Table 5 for wild-type and GAL2 mutant, as defined by the 5D and 9D models. Fig. B3 shows that an increase in the frequency leads to a low decrease in the baseline and to a prominent decrease in the amplitude of the output signals G_1 and M_1. The figure also shows that there is little variation between the reported results for the two model strains, on the order of 10^{-5} for the baseline and the phase difference and 10^{-6} for the normalized amplitude (see Table 5). One of these results is qualitatively consistent with that of Bennett et al. (2008) showing that the GAL network can low-pass filter glucose, the repressor of the network, by decreasing both the amplitude and the phase of the output signal when increasing the frequency of the glucose input signal. Although the models presented here can produce one aspect of this low-pass filtering capacity (namely, the decrease in amplitude), they cannot reproduce the decrease in the phase shift at high frequencies (see Fig. B3 (B) of Appendix B). Indeed, our simulations show that at high frequencies, the system responds rapidly to glucose and peaks earlier when responding to low frequencies.

A possible source for this discrepancy between our results and the reported experimental data is the method employed for calculating the phase difference; Bennett et al. (2008) used recorded inputs to calculate phase shifts, which often appear to drift upward and exhibit a decrease in amplitude. These two issues may, as a result, affect the peaks of the input and the overall phase shift values (reported to vary between 0 and $-3\pi/2$ in experimental settings). For our simulation, we used a pure sinusoidal for the glucose oscillatory signal and calculated the input and output phases using the Hilbert transform (as shown in Table 4). For such an input signal, the phase shift occurs between $[-\pi, -\pi/2]$ (see Table 5), and no decrease in the phase difference is observed, as stated earlier. We do observe, however, similar results when using the same pure sinusoidal input signal applied to the model of Bennett et al. (2008). These results suggest that the galactose network does not filter out repressor fluctuations of high frequencies but rather adapts by oscillating with a low amplitude.

To assess the similarity of the output signal to the pure sinusoidal input signal used in our simulation, we measure the upstroke and the downstroke fractions of the cycle, as defined in Table 4. Table 5 and Fig. B3(C) (in Appendix B) show that although the wild-type and the GAL2 mutant strains, defined by the 5D and 9D models, exhibit similar characteristics, the 5D model produces a stable 55:45 ratio between the downstroke and the upstroke phases of the cycle for all frequencies, but the 9D model gradually shifts this ratio from 1:1 to 55:45 as the frequency is increased.

Table 5
The properties of the 5D and the 9D models (with n=1), for both the wild type (WT) and the GAL2 mutant yeast strains. The values for the baselines and amplitudes of the oscillations are the same within the first two decimal places. The phase difference between the input–output signals (glucose-G_1 for the 5D model, and glucose-M_1 for the 9D model) also showed a striking similarity between the two types of strain. The upstroke phase of the oscillations occupied a smaller percentage than the downstroke phase, decreasing with increasing frequency for both strains.

Measures	Model	Yeast type	Period of the input signal (bold) [h]					
			4.5	**3.0**	**2.25**	**1.5**	**1.125**	**0.75**
Normalized baseline	5D	WT/GAL2Δ	1.00	1.00	0.99	0.99	0.99	0.99
	9D	WT/GAL2Δ	1.00	0.99	0.98	0.97	0.97	0.96
Normalized amplitude	5D	WT/GAL2Δ	1.00	0.68	0.51	0.34	0.26	0.17
	9D	WT/GAL2Δ	1.00	0.90	0.80	0.63	0.51	0.36
Phase difference (ϕ_i) [rad]	5D	WT/GAL2Δ	−1.80	−1.74	−1.68	−1.65	−1.64	−1.62
	9D	WT/GAL2Δ	−2.69	−2.53	−2.38	−2.17	−2.05	− 1.90
Upstroke percentage of oscillations [%]	5D	WT	45.01	44.83	44.818	44.778	44.74	44.73
	5D	GAL2Δ	45.02	44.83	44.81	44.67	44.74	44.67
	9D	WT	49.07	48.06	47.26	46.22	45.63	45.33
	9D	GAL2Δ	49.07	48.06	47.33	46.33	45.63	45.33

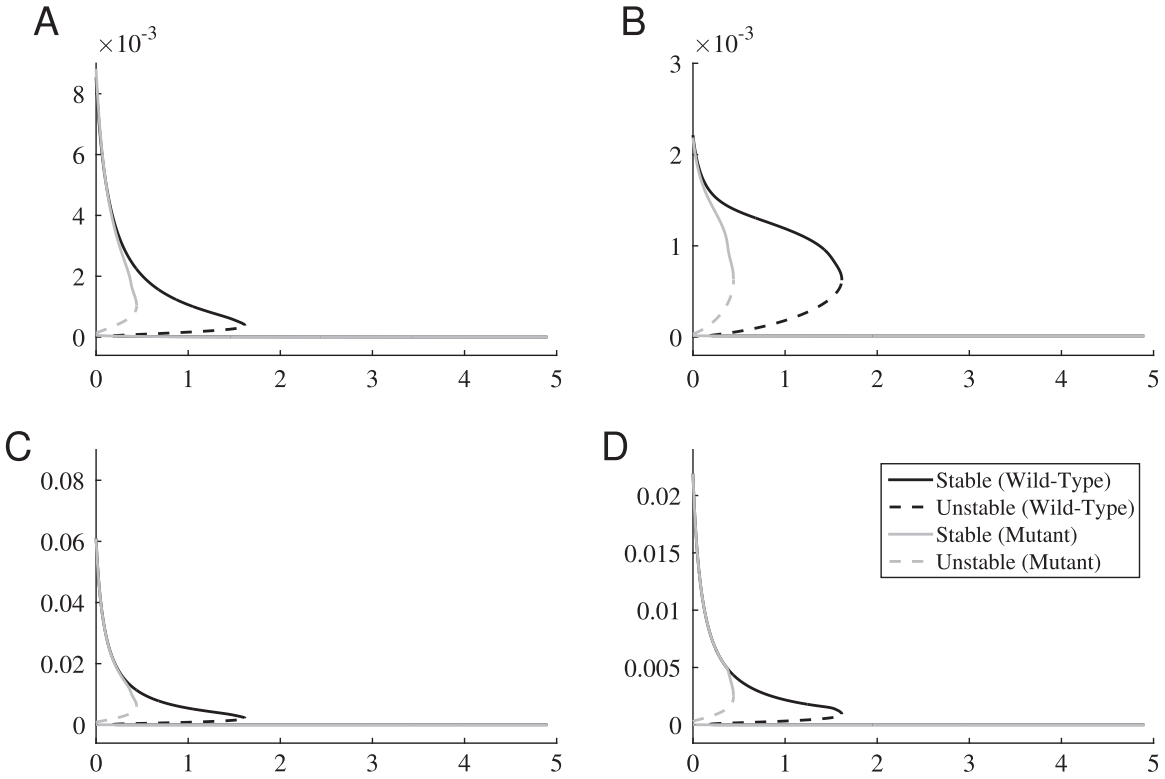

Fig. 6. One-parameter bifurcation of GAL proteins as a function of glucose (R), measured in units of [% w/v]. The four panels show the steady state values of (A) the regulatory protein Gal3 (G_3); (B) the inhibitory regulatory protein Gal80 (G_{80}); (C) the permease Gal2 (G_2); and (D) the regulatory and enzymatic protein Gal1 (G_1). Solid lines represent the stable branches of attracting equilibria, whereas dashed lines represent the unstable branches of equilibria, for both wild-type (black) and GAL2 mutant (grey) yeast strains.

Although the two models eventually reach the same ratio at high frequencies, the adaptive behaviour of the 9D model at low frequency is likely to be due to the presence of slow rates in the model providing it with more time to adapt to an idealized sinusoidal signal.

In the simulations above, the amplitude of the input signal is kept fixed. To investigate how altering the amplitude of glucose oscillatory signal affect the response of the GAL network, we plot in Fig. B4 of Appendix B, the amplitude of the output signal M_1 with respect to the amplitude of R. Our results reveal that these two amplitudes are positively correlated, and that their correlation can be best fit by a quadratic polynomial (a prediction that can be verified experimentally).

3.2.4. *Bistability with respect to glucose*

As suggested in Section 2.3, glucose acts as a repressor of the GAL network through four independent processes: (i) by increasing the dilution rate μ, (ii) by enhancing vesicle degradation of the G_2 transporter, (iii) by repressing the transcription of GAL3, GAL1 and GAL4, and (iv) by competing with galactose to bind with G_2. These processes have been all included in the 9D model described by Eqs. (21a–i). To analyze the relation between the dynamical properties of the model and the oscillatory input signals, we plot the bifurcation diagrams of the various Gal proteins with respect to glucose for both the wild-type and the GAL2 mutant strains (Fig. 6). Bistability in the expression level of G_3 (panel A), G_{80} (panel B), G_2 (panel C) and G_1 (panel D) is observed in all cases at low values of glucose, whereas monostability (determined by the uninduced state) is only observed in one regime at intermediate to high values of glucose. Interestingly, these panels show that although a decrease in the induced (upper) stable branch is observed during an increase in glucose, they remain slightly more elevated than the non-induced (lower) branch at the limit point.

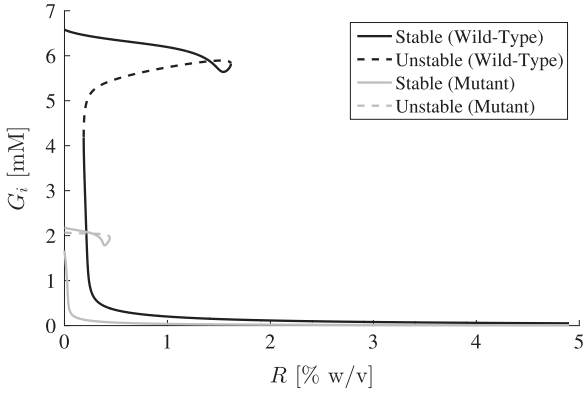

Fig. 7. One-parameter bifurcation of intracellular galactose concentration (G_i) with respect to glucose (R), for both wild-type (black) and GAL2 mutant (grey) yeast strains. As before, solid and dashed lines define the stable and unstable branches, respectively.

The switch from the non-induced to the induced stable branch at the limit point is consistent with that seen experimentally in the level of GAL1 induction (Bennett et al., 2008).

Plotting the bifurcation diagram of intracellular galactose (G_i) with respect to glucose in Fig. 7, we observe a fold around the right limit point situated at about 1.8% w/v glucose. This feature is likely due to the multidimensionality of the system. Unlike the bistability of Fig. B1, Fig. 7 shows a large difference between the induced state and the uninduced state inside the bistable regime, an outcome that should be testable experimentally. The steep increase in G_i seen in the uninduced state inside the bistable regime is analogous to the sharp increase in the Gal protein expression, especially G_2, seen in the induced states of Fig. 6.

Recall that the GAL2 mutant strain is simulated by decreasing

the transport rate α. This causes the induced stable branch to shift downward for all GAL components, as seen in Fig. 6. The shape of the bifurcation diagram in Fig. 7 can be used to explain how narrowing down of the bistability regime affects the output response to glucose periodic forcing. Given that the uninduced stable branches are similar for both strains, we expect the system in both cases to tend to the noninduced stable branch, if the initial conditions are low. Therefore, narrowing down the bistability regime by decreasing α does not affect the properties of the oscillations during glucose periodic forcing because of the presence of peaks in the input signal (causing significant repression in the expression level of the GAL proteins) and the ability of the network to adapt quickly. An additional prediction from our model is that if the glucose oscillatory input signal is varied between 0 and 3% w/v, the galactose network would cross the right limit point of the bifurcation diagrams shown in Figs. 6 and 7 and as a result shift back and forth between the bistable and monostable regimes.

4. Discussion

In this study, we have shown that the bistability property of the GAL regulon, originally seen in a model of Apostu and Mackey (2012) is still preserved in improved models of the galactose network. These new models consider additional regulatory and metabolic processes not previously accounted for, including (i) the dimerization of regulatory proteins, (ii) the existence of multiple upstream activating sequences at the level of the promoter and (iii) the metabolic reactions involving galactose and glucose repression processes. The results produced by the models were qualitatively in agreement with those seen in Apostu and Mackey (2012), and quantitatively in agreement with those seen in Ideker et al. (2001) and Sellick et al. (2008).

In this study, we combined various features of previous studies in our modeling approach and used the *in vivo* results of Abramczyk et al. (2012), that showed the localization, outside and inside the nucleus, of the tripartite complexes G_4: G_{80}: G_3 and G_4: G_{80}: G_1, acting as transcription factors. Our goal was to decipher the dynamics of the GAL network, by including both the short and the long-term complexes in our modeling construct.

The models developed here contain a minimalistic metabolic branch interacting with a regulatory gene network. Using these models, we were able to explain the response of the system to periodic forcing by glucose, and show that this network is robust to changing environments and nonhomeostatic conditions. The models also revealed that large discrepancies between responses of different strains or cells can be generated by decreasing the transport rate α or by drastically altering the external glucose and galactose conditions.

In the models developed here, we did not include the regulatory protein Gal4 and the metabolic enzymes Gal7p and Gal10p for various reasons. First, as it has been already mentioned in Apostu and Mackey (2012), the expression level of Gal4 protein is not affected when cells are transferred from raffinose to galactose medium (Sellick et al., 2008). As for the metabolites generated due to the downstream enzymes Gal7p and Gal10p, they do not feedback into the gene network and their respective negative feedback processes are represented in our model through the phosphorylation rate of galactose by the Gal1p kinase. Limiting the number of dynamical equations to the ones involving the key proteins has allowed us to gain a better understanding of how the different molecular constituents interact at the level of the regulon.

The main goal of this study is to determine how the feedback loops of the whole network interact together to form emergent behaviour under various experimental conditions. Using bifurcation analysis, we demonstrated that bistability persists in the full model and plays an integral part in the dynamics of the network. It is affected by most variables (except for intracellular galactose) and underlies many of the features observed experimentally (including the binary response). We also showed that galactose transport into the cell is the main rate limiting step in the Gal network induction.

A natural question is whether bistability could play a role in galactosemia. Potential causes for this disease have already been found, mostly in association with genetic mutations that cause accumulation of galactitol in various tissues. From a mathematical point of view, one can study this disease via parameter perturbations that can lead to an increase in the activation of some reverse rates and a decrease in the accumulation of harmful metabolites. One interesting prediction of our model is that the half-maximum activation of the transport (K) is the main parameter that controls the minimal galactose concentration required for bistability (see Fig. 3(F)). By translating the bistable regime to larger concentrations of extracellular galactose (i.e., to the right of the current bifurcation diagram), greater values of K would reduce the likelihood of the organism to be fully induced at small galactose concentrations. Altering this constant experimentally, perhaps by blocking or modifying the transporter, would decrease the amount of galactitol, the toxic metabolite. A natural continuation of the present work would be to try to describe a threshold for the toxic levels of galactose and its other metabolites, in the context of this disease, particularly during accumulation of Gal1P (Gitzelmann, 1995).

Another property of the system deduced from our mathematical models is the interplay between the repressor and the inducer of the galactose network. The bifurcation diagrams plotted with respect to glucose (Figs. 6(A)–(D) and 7) show that a high glucose level impedes galactose accumulation, which in turn decreases Gal1P level. An experimental protocol similar to the ones employed in van den Brink et al. (2009) or Acar et al. (2005) can verify our predictions, by measuring the levels of Gal1P for different combinations of galactose and glucose concentrations. Although the two monosaccharides (glucose and galactose) are processed differently, a combination of the two pathways can be beneficial for the yeast cells whose metabolic machinery is not properly functional.

The lack of experimental data has made our modeling effort a challenging one, relying mostly on estimation techniques. To further validate the models against experimental data, our assumptions on transcriptional repression and competition for the Gal2p transporter due to glucose concentration should be tested experimentally. In the models, we have described the effects of the repressor by Michaelis–Menten type functions whose parameters were estimated using the Genetic Algorithm (see Appendix A). To assess our predictions, experiments can follow the procedures of Barros (1999), to measure sugar transport, and of Lashkari et al. (1997), to obtain mRNA fold-difference values in cells grown in different galactose and glucose mixtures.

The complexity of this network makes the use of mathematical models an alternative and a promising tool to decipher its kinetics. The rapid discovery of new pathways adds more emphasis on the importance of using such modeling approaches to accomplish this goal. The incorporation of new pathways into the models will allow us to study their effects, including their role in stabilizing/destabilizing the steady states of the model and in defining adaptability to environmental perturbations. It will also allow us to predict emergent behaviour exhibited by the model and determine their effects on the physiology of the network.

Acknowledgements

This work was supported by grants to Anmar Khadra and Michael C. Mackey from the Natural Sciences and Engineering Research Council (NSERC).

Appendix A. Parameter estimation and software

A.1. Measured parameters

- *Conversion factor* (c): Although there is a large variation in the shape of yeast cells and their volume we consider the generic yeast cell to be spherical, haploid cell, of volume 70 μm^3. This value has been published in Sherman (2002) and has been used in other computational models (Ramsey et al., 2006; Apostu and Mackey, 2012).
  The cellular volume and Avogadro's number are two constants required for estimating c, defined to be the conversion constant in Table 1. This parameter is included to maintain the consistency of units between [mM] and [molecules/cell], and is given by

$$1\ \text{mM} = \frac{10^{-3}\ \text{mol}}{1\ \text{L}} = \frac{6.02214129 \times 10^{23} \times 10^{-3}\ \text{molecules}}{(1\ \text{dm})^3}$$
$$= \frac{6.02214129 \times 10^{20}\ \text{molecules}}{(10^{-5}\ \mu\text{m})^3} \times \frac{70\ \mu\text{m}^3}{\text{cell}}$$
$$= 4.2154989 \times 10^{7}\ \text{molecules/cell} = c.$$

- *Conversion factor* (c_g): Sugars are usually administered in concentrations of [% w/v], whereas the half-maximum activation constant for the galactose transport (K) is given in mM. Therefore, we use the conversion factor c_g, given by

$$1\%\text{w/v} = \frac{1\ \text{g}}{100\ \text{mL}} = \frac{1\ \text{g}}{0.1\ \text{L}} \frac{1\ \text{mol}}{180.56\ \text{g}} = \frac{10^3\ \text{mmol g}}{180.56\ \text{g}\cdot 0.1\ \text{L}}$$
$$= \frac{10^4}{180.56}\ \text{mM} = c_g \tag{A.2}$$

  to maintain consistency with Eq. (13).
- *Dilution rate* (μ): The dilution rate is often calculated by using the doubling time of the cells. Ramsey et al. (2006) and Apostu and Mackey (2012) used a doubling time of 180 mins in their models, which is equivalent to 3.85×10^{-3} min^{-1}. However, to obtain consistency between our parameter choices for modelling glucose repression, we averaged of the doubling rates reported by Tyson et al. (1979), to obtain 156 min in galactose and 79 min in glucose. Based on the above, we conclude that

$$\mu_a = \frac{\ln 2}{156\ \text{min}} \approx 4.438 \times 10^{-3}\ \text{min}^{-1},$$
$$\mu(R)_{max} = \mu_a + \mu_b = \frac{\ln 2}{79\ \text{min}} \approx 5.12 \times 10^{-3}\ \text{min}^{-1}.$$

- *mRNA degradation rate* (γ_M): This parameter has been measured experimentally as the half life-time of the mRNA strands. Wang et al. (2002) measured this quantity for an average strand, whereas Bennett et al. (2008) measured it for GAL3 and GAL1. We have approximated the half-life time at 16 min, which is equivalent to

$$\gamma_M = \frac{\ln 2}{16\ \text{min}} \approx 43.32 \times 10^{-3}\ \text{min}^{-1}.$$

- *Protein degradation rates* ($\gamma_{G,i}$, $i \in \{3, 80, 2, 1\}$): The values were initially measured in Holstege et al. (1998) and Wang et al. (2002) and used in the model developed by Ramsey et al. (2006). Here, we use the same parameters as in Ramsey et al. (2006), except that the protein degradation in our model does not represent the degradation arising from cellular growth, but rather from protein processing only. This implies that

$$\gamma_{G,3} = 11.55 \times 10^{-3}\ \text{min}^{-1} - 4.438 \times 10^{-3}\ \text{min}^{-1}$$
$$= 7.112 \times 10^{-3}\ \text{min}^{-1},$$
$$\gamma_{G,80} = 6.931 \times 10^{-3}\ \text{min}^{-1} - 4.438 \times 10^{-3}\ \text{min}^{-1}$$
$$= 2.493 \times 10^{-3}\ \text{min}^{-1},$$
$$\gamma_{G,2} \approx 0\ \text{min}^{-1},\ \gamma_{G,1} \approx 0\ \text{min}^{-1}.$$

- *Transcription rates* ($\kappa_{r,3}$, $\kappa_{r,80}$, $\kappa_{r,2}$, and $\kappa_{r,1}$): Transcription rates are estimated using similar approach to that presented by Apostu and Mackey (2012). More specifically, they are approximated by using mRNA steady state ratios, measured in cells grown in induced versus repressed extracellular media. In other words, their numerical values ($\kappa_{r,i}$, $i = 3, 80, 2, 1$) are calculated by setting Eqs. (6), (8), (10) and (12a), describing the dynamics of mRNA, to 0, and solving for $\kappa_{r,i}$ in terms of the steady state values $M_{i,(ss)}$ as follows:

$$\kappa_{r,i} = M_{i,(ss)} \frac{\gamma_M + \mu_a}{100\%}, \quad i \in \{3, 80, 2, 1\}.$$

  The mRNA steady state levels in glucose were estimated in Arava et al. (2003) to be 0.8, 1.1 and 1.0 molecules/cell for GAL3, GAL80 and GAL1, respectively. Since there are no estimates available for the steady state level of Gal2p, we used instead the steady states of mRNAs for all hexose transporters reported by Arava and colleagues. Table 3 in the appendix of Arava et al. (2003) contains the copy numbers for 17 hexose transporters. We use all these values, except for one that is particularly high (5 compared to a range of [0.2, 2.6] for the other hexose copy numbers values) to calculate the median, which gives the approximate value of 0.598 mRNA copies/cell.
  To calculate the transcription rates in galactose, we also consider the fold difference between mRNA values in galactose-grown compared to glucose-grown cells, as reported by Lashkari et al. (1997). Based on this premise, we have

$$\kappa_{r,i} = \text{mRNA}_{\text{level in glucose}} \times \text{Fold number} \times (\gamma_M + \mu_a)$$
$$\kappa_{r,3} = 0.8\ \text{molecules/cell} \times 8.6 \times (4.78 \times 10^{-2}\ \text{min}^{-1})$$
$$= 0.329\ \text{molecules/(cell} \times \text{min)}$$
$$\kappa_{r,2} = 0.598\ \text{molecules/cell} \times 23.7 \times (4.78 \times 10^{-2}\ \text{min}^{-1})$$
$$= 0.678\ \text{molecules/(cell} \times \text{min)}$$
$$\kappa_{r,1} = 1.0\ \text{molecules/cell} \times 21.8 \times (4.78 \times 10^{-2}\ \text{min}^{-1})$$
$$= 1.042\ \text{molecules/(cell} \times \text{min)}$$
$$\text{Upper bound of } \kappa_{r,80} = 1.1\ \text{molecules/cell} \times 3.0 \times (4.78 \times 10^{-2}\ \text{min}^{-1}) = 0.158\ \text{molecules/(cell} \times \text{min)}$$
$$\text{Lower bound of } \kappa_{r,80} = 1.1\ \text{molecules/cell} \times 2.8 \times (4.78 \times 10^{-2}\ \text{min}^{-1}) = 0.147\ \text{molecules/(cell} \times \text{min)}.$$

- *Translation rates* ($\kappa_{l,3}$, $\kappa_{l,80}$, $\kappa_{l,2}$, and $\kappa_{l,1}$): The four parameters associated with the transcription rates of GAL3, GAL80, GAL2 and GAL1 are not measured experimentally using the desired units and the sugar medium that we require for the model. Arava et al. (2003) presented in Table 3 of their supplementary information the protein synthesis rates in glucose media for an extensive list of mRNA strands, in units of [proteins/s]. Since we are interested purely in the translation rates $\kappa_{l,i}$ ($i = 3, 80, 2, 1$), in units of [proteins/mRNA copies × cell], we estimate these parameters based on the following equation:

$$\kappa_{l,i} = \frac{\text{Fraction of translated mRNA} \times \text{Elongation rate}}{\text{Protein length}} \times \frac{\text{Number of proteins}}{\text{mRNA}}, \tag{A.6}$$

where the "fraction of translated mRNA" is assumed here to be equivalent to the "relative translation rate", defined in Arava et al. (2003) to be

Relative translation rate = Ribosome occupancy × Ribosome density.

For this relation, the ribosome occupancy is approximated by the ribosomal mRNA level divided by the total mRNA level of that species available in the cell, and the ribosome density is given by the number of ribosomes per length of unit of the open reading frame. The relative translation rate, calculated in this manner in Arava et al. (2003), is therefore dimensionless and is given by 0.143, 0.039 and 0.042 for GAL3, GAL80 and GAL1, respectively. For GAL2, the lack of experimental data constrains us to use the median relative translation rates of all associated GAL mRNAs reported, which is given by 0.145.

As for value of the mRNA elongation rate, it was reported in Arava et al. (2003) to be 10 amino acids (a.a.) per second, for the yeast cells grown in YPD medium (i.e., 1% yeast extract, 2% peptone and 2% dextrose). This rate is similar to that obtained by Bonven and Dullov (1979), who found that is about 9.3 a.a per second for budding yeast grown in glucose instead of a mix of peptone and dextrose.

To calculate the translation rates of Eq. (A.6), we still need the length of the protein, measured in number of amino acids, and the ratio of proteins to mRNA. We already know that Gal proteins measure: 520, 435, 528, and 574 amino acids (for Gal3p, Gal80p, Gal1p and Gal2p, respectively). Furthermore, Ideker et al. (2001) found that the ratios of proteins to mRNA lies between 4200 and 4800. Based on the above observations, we can now calculate the translation rates of Eq. (A.6) as follows:

Lower bounds:

$$\kappa_{l,3} = \frac{0.143 \times 9.3 \times 60 \text{ a. a./ min}}{520 \text{ a. a}} \times 4200 \frac{\text{Proteins}}{\text{mRNA}} = 644.49 \frac{\text{Proteins}}{\text{mRNA} \times \text{min}}.$$

$$\kappa_{l,80} = \frac{0.039 \times 9.3 \times 60 \text{ a. a./ min}}{435 \text{ a. a}} \times 4200 \frac{\text{Proteins}}{\text{mRNA}} = 210.12 \frac{\text{Proteins}}{\text{mRNA} \times \text{min}}.$$

$$\kappa_{l,1} = \frac{0.042 \times 9.3 \times 60 \text{ a. a./ min}}{528 \text{ a. a}} \times 4200 \frac{\text{Proteins}}{\text{mRNA}} = 186.42 \frac{\text{Proteins}}{\text{mRNA} \times \text{min}}.$$

$$\kappa_{l,2} = \frac{0.145 \times 9.3 \times 60 \text{ a. a./ min}}{574 \text{ a. a}} \times 4200 \frac{\text{Proteins}}{\text{mRNA}} = 592.02 \frac{\text{Proteins}}{\text{mRNA} \times \text{min}}.$$

We have used these lower bounds for the translation rates, as shown in Table 1.

- *Dimerization constants*: Melcher and Xu (2001) reported that the dimerization constant for $G_{80,d}$ ($K_{D,80}$) is 1 to 3×10^{-7} mM. In our model simulations, we used the upper bound.
- *Dissociation constants* ($K_{B,80}$ *and* $K_{B,3}$): The dissociation constant of the Gal80p dimer from the promoter conformation D_2 is measured to be 3×10^{-8} mM, in Melcher and Xu (2001), and 5×10^{-6} mM, in Lohr et al. (1995). The dissociation constant of the activated Gal3p from the Gal80p molecule was numerically estimated by Venkatesh et al. (1999) to be 6×10^{-8} mM. We use this latter value to estimate the dissociation constant $K_{B,3}$. This value represents the rate of a single G_{80} binding to an activated G_3 molecule in the cytoplasm, in the context of a different kind of GAL model (i.e., based on nucleo-cytoplasmic shuttling of G_{80}). In our model, however, we consider the reaction between dimers of each of these species, not single molecules. Due to the lack of relevant data we still use these values as an approximation and set

$$K_{B,80} = 5 \times 10^{-6} \text{ mM}, \quad K_{B,3} = 6 \times 10^{-8} \text{ mM}.$$

- *Transport rate* (α): For the transport rate, we use, as a reference, the value 4350 min^{-1} provided in de Atauri et al. (2005). The authors of this latter study mention that the rate was adjusted in order to obtain a V_{max} consistent with that observed experimentally in Reifenberger et al. (1997).
- *Parameters involved in galactose phosphorylation* (κ_{GK}, K_m, K_{IC}, K_{IU}): The rate parameters associated with phosphorylation have been previously estimated in the experimental paper of Timson and Reece (2002). No other manipulations and calculations are necessary, since the units and the definitions of all rate constants are in agreement with the ones used in our models (see Table 1).
- *Metabolic rate* (δ): A suitable candidate for estimating this parameter is the rate of the reaction catalyzed by the Gal7p transferase enzyme, which ensures that Gal-1-Phosphate is metabolized and incorporated into the glycolytic pathway. This catabolic rate of the transferase ($k_{cat,GT}$) has been measured as 59,200 min^{-1} and used in the study of de Atauri et al. (2005). Thus we set

$$\delta \approx k_{cat,GT} = 59,200 \text{ min}^{-1}.$$

A.2. Parameters estimated through the model

- *Half-maximum activation of* G_3 *and* G_1 (K_S): It has been known for some time that galactose induces the entire regulatory system via the activation of Gal3p molecule, but the actual reactions involved in this induction process remain incompletely understood. Several modelling papers focusing on this topic have assumed that this process follows either Michaelis–Menten activation kinetics (Venkatesh et al., 1999), similar to the formalism used here, or linear kinetics (Acar et al., 2005; de Atauri et al., 2005). This process is also modelled in terms of a positive constant added to the rates of change of the different proteins induced by galactose (Venturelli et al., 2012).
  Given that a Michaelis–Menten formalism has been used to describe activation, the value of half-maximum activation of these reactions is assumed to be identical to the estimated numerical value of 4000 mM, given in Apostu and Mackey (2012). By having a very large half-maximum activation, we are assuming an almost-linear relationship between the concentrations of activated Gal3 and Gal1 proteins and the intracellular galactose, which would be in agreement with other modelling papers that have used a direct proportional (or linear) relationship.
- Parameters of the regulatory pathways involving Gal3p and Gal1p ($k_{cat,3}$, $K_{D,3}$, $k_{cat,1}$, $K_{D,1}$ and $K_{B,1}$): As indicated earlier, the process of Gal3p and Gal1p activation is not fully understood. By using QSS assumption on the model, we can derive relations between the different parameters of the model based on its steady states.
  According to Eq. (5), we have

$$K_3 = \frac{\sqrt{K_{D,3}K_{B,3}}(\gamma_{G,3} + \mu)}{\kappa_{C,3}}$$

$$K_1 = \frac{\sqrt{K_{D,1}K_{B,3}K_{B,1}}(\gamma_{G,1} + \mu)}{\kappa_{C,1}}.$$

Due to the fact that bistability is one of the main properties of

the GAL network (observed within a given physiological range of galactose concentration), one can use this property to numerically estimate the two parameters K_3 and K_1. In other words, the values of these parameters can be determined by ensuring that the model can produce bistability. Based on this, we find that $K_3 = 1.729 \times 10^{-6}$ mM^2 and $K_1 = 3.329 \times 10^{-6}$ mM^2. Since we already know the degradation rates, the dilution rates for these proteins as well as the activation rate $K_{B,3}$, we can solve for the following ratios in term of the parameters $K_{D,i}$, $K_{B,1}$, $\kappa_{C,i}$:

$$\frac{\sqrt{K_{D,3}}}{\kappa_{C,3}} = \frac{K_3}{\sqrt{K_{B,3}}(\gamma_{G,3}+\mu)} = 4.363 \times 10^{-3}\ \text{mM}^{1.5}\ \text{min}$$

$$\frac{\sqrt{K_{D,1}K_{B,1}}}{\kappa_{C,1}} = \frac{K_1}{\sqrt{K_{B,3}}(\gamma_{G,1}+\mu)} = 3.062\ \text{mM}^{1.5}\ \text{min}.$$

These ratios are used in the functions K_3 and K_1

$$K_3 = \sqrt{K_{B,3}}(\gamma_{G,3}+\mu) \times 4.363 \times 10^{-3}\ \text{mM}^{1.5}\ \text{min}$$

$$K_1 = \sqrt{K_{B,3}}(\gamma_{G,1}+\mu) \times 3.062\ \text{mM}^{1.5}\ \text{min}.$$

A.3. Numerical estimation of parameters

- Software
  The numerical results that we have presented in the main text were obtained using two main software packages: XPPAUT (written by Bard Ermentrout and freely available online), used for numerical bifurcation analysis, and MATLAB (MathWorks Inc., 2014, Natick, Massachusetts), used for simulating the differential equation models. "cftool" and "ga" toolboxes available in MATLAB were used to fit various expressions to experimental data as explained below.
- Data fitting
  - *Parameter estimation using "Cftool"*: As shown in Fig. A1 and Table A1, the half-maximum activation for the repressive functions characterizing the dilution and Gal2p degradation rates are estimated using Michaelis–Menten functions in the "Cftool" toolbox (with $R=1$, SSE = 5.5×10^{-14} for the dilution rate, and $R=1$, SSE = 1.12×10^{-14} for the degradation rate).

Table A1
Parameter values associated with dilution and GAL2 degradation obtained using a combination of parameter estimation and "Cftool" fitting.

Processes	Expression	Parameters	Value	Reference
Dilution	$\mu(R) = \mu_a + \frac{\mu_b R}{\mu_c + R}$	μ_a	4.44×10^{-3}	Tyson et al. (1979)
		$\mu_a + \mu_b$	8.78×10^{-3}	Tyson et al. (1979)
		μ_c	5.12×10^{-3}	Fitted with "Cftool"
G_2 Degradation	$\gamma(R) = \gamma_{G,2} + \frac{\gamma_b R}{\gamma_c + R}$	$\gamma_{G,2}$	3.98×10^{-3}	Horak and Wolf (1997)
		$\gamma_{G,2} + \gamma_b$	7.66×10^{-3}	Horak and Wolf (1997)
		γ_c	1.416×10^{-3}	Fitted with "Cftool"

This toolbox is also used to estimate the phase of the glucose oscillatory inputs administered in the experiments of Bennett et al. (2008). This was done by digitizing the data presented in the first rows of panels A and B in Figure Fig. 3 of that paper and fitting each outcome to a sinusoidal signal with a given period. The baseline was allowed to vary during this process.

  - *Parameter estimation using the Genetic Algorithm*: The parameters associated with the transcriptional repression and competition for the G_2 transporter (x_b, y_b, y_c) are estimated using the Genetic Algorithm. This was done by minimizing the error between the experimental data and the steady state values of the extended 5D and 9D models. Rates of transcriptional repression and galactose transport are both modelled as Hill functions with negative coefficients and fitted to data from Bennett et al. (2008) (see Fig. A2). Since the type of inhibition in these processes is unknown, the Hill coefficients are left undetermined and allowed to assume only two values: either 1 or 2. The latter follows from the fact that trimer complexes are far less likely to form than monomers and dimers. The results from this optimization technique, along with the error estimate, are presented in Table A2 shown below.

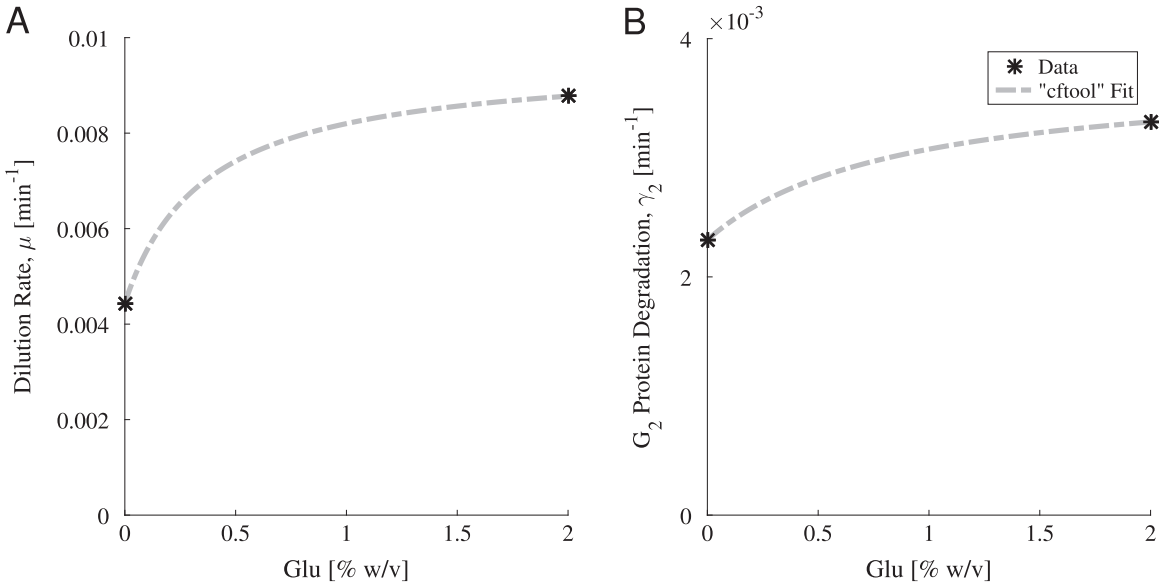

Fig. A1. Cellular processes affected by glucose. (A) An increase in glucose concentration leads to an increase in the dilution rate (μ). (B) An increase in extracellular glucose induces an increase in the degradation rate of the transporter protein G_2 (γ_2). Black asterisks represent experimental data obtained from Tyson et al. (1979) and Horak and Wolf (1997), whereas dashed grey lines represent the fitted Michaelis–Menten functions using the "Cftool" toolbox in MATLAB.

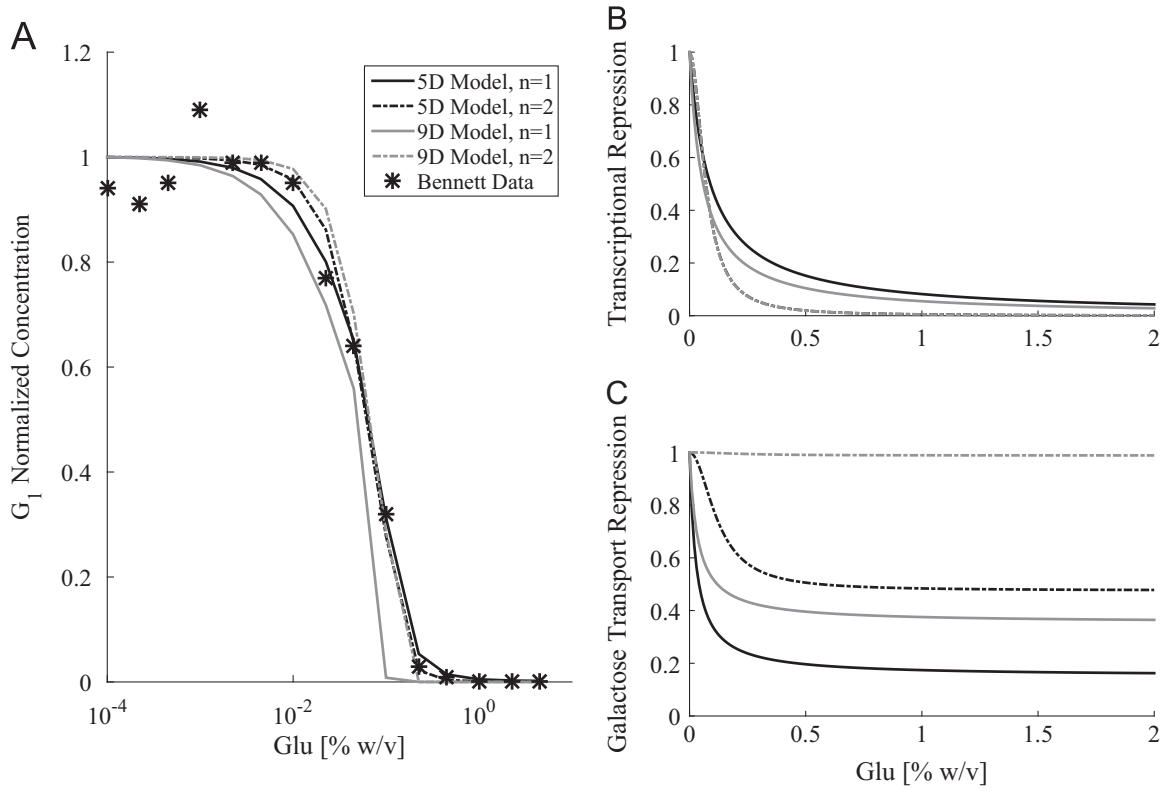

Fig. A2. Data fitting of glucose-induced repression. (A) Experimental data published by Bennett et al. (2008) for the normalized G_1 concentration, shown in asterisks, was used to estimate the parameters of the Hill functions for the repressor processes in the extended 5D and 9D models (black and grey lines, respectively). These Hill functions were allowed to have a coefficient of 1 and 2 (solid and dashed lines). (B) The half-maximum deactivation is similar for the four fitted models. (C) Transport of galactose through the G_2 permease is also decreased due to the presence of the repressor. The four models behave differently here, with large variations in the half-maximum deactivation and the asymptotic minimum.

Table A2
Parameter values associated with the two processes transcriptional repression (by glucose) and competition for the transporter, as determined by the Genetic Algorithm. Parameter combinations that were used in Section 3 are shown in bold.

Value of *n*		**5D**		**9D**	
		1	**2**	**1**	**2**
Half-maximum transcriptional repression	x_c	**0.2443**	2.4107	**0.2657**	0.0650
Transport competition rate	y_b	**0.0003**	0.5639	**0.4950**	0.4950
Half-maximum transport competition	y_c	**2.9989**	0.0052	**2.3142**	2.3142
Error estimation		**0.0387**	0.0300	**0.0876**	0.1402

- *Hilbert transform*: The Hilbert transform allows one to calculate the phase and the amplitude of an oscillatory signal, $u(t)$. In theory, it convolves the signal with the Cauchy kernel, also known as Cauchy Principal value (*p.v.*), given by

$$p.\,v.\,(f(x)) = \lim_{a\to\infty}\int_{-a}^{a} f(x)dx,$$

where $f(x)$ is a function with the properties

$$\int_{-\infty}^{0} f(x)dx = \pm\infty \quad \text{and} \quad \int_{0}^{\infty} f(x)dx = \mp\infty.$$

This type of improper integral is used in the calculation of the

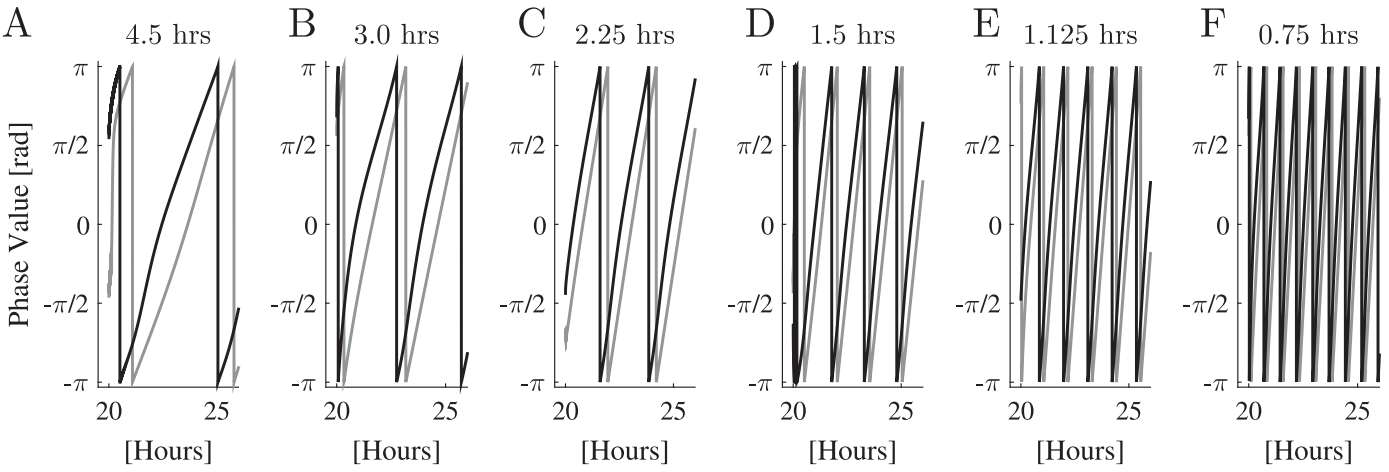

Fig. A3. Hilbert transform of the oscillatory glucose input and the G_1 output signals, showing the periodicity of both signals and their phase characteristics. (A)–(F) Glucose (grey lines) and the galactokinase G_1 (black lines) oscillatory signals at steady state (i.e., after 20 h) exhibiting at least one cycle. The output signal follows the input signal very closely and adapts to its periodicity given by (A) 4.5, (B) 3, (C) 2.25, (D) 1.5, (E) 1.125 and (F) 0.75 h.

Hilbert transform defined by

$$H(u(t)) = \frac{1}{\pi} p.v. \int_{-\infty}^{\infty} \frac{u(\tau)}{(t-\tau)} d\tau.$$

One of the properties of this transform is that it shifts the signal within the integral by $\pi/2$, i.e. $H(H(u))(t) = -u(t)$. It is also related to the Fourier transform by the relation

$$F(H(t)) = F\left(\frac{1}{\pi t}\right) F(u(t)).$$

In discrete form, the Hilbert transform can be calculated in MATLAB, using the function 'Hilbert'. This function computes the transform by generating a complex signal $H(u(t)) = A(t)e^{i\phi(t)}$ from the original signal $u(t)$. The complex signal is then used to evaluate its amplitude (A) and phase (φ) based on the equations

$$A(t) = \mathcal{R}e(H(u(t)))$$
$$\varphi(t) = angle(H(u(t))),$$

where $\mathcal{R}e$ is the real part of the Hilbert transform and *angle* is a predefined MATLAB function for the instantaneous phase of the transform within $(-\pi, \pi)$. This method was also used in Khadra (2009) to analyze synchrony in a population of synchronized neurons.

As an example of the Hilbert transform technique of calculating the phase of a signal, we will refer to Fig. A3 shown below, containing the estimated phase difference between the oscillatory glucose input signal and G_1 output response for the wild-type strain, using the GAL extended 5D model, with $n=1$. This calculation involves applying the Hilbert Transform on both the glucose input and the Gal1p output signals. Notice how the output signal (black lines) follows the input (grey lines), but the lines are not always straight, due to the fact that the output is not purely sinusoidal.

Appendix B. Additional derivations and results

B.1. Analytical derivations

- *Rates of change for the activated proteins G_3^* and G_1^**: The activated forms of the Gal3 and Gal1 proteins are produced based on Eq. (1), and subject to protein degradation, similar to the species G_3, G_{80}, G_2 and G_1 (see (Eqs. (7), (9), 12b) and (11)). Thus, we can write

$$\frac{dG_3^*}{dt} = G_3 F_3(G_i) - \left(\gamma_{G,3} + \mu\right) G_3^* \tag{B.1a}$$

$$\frac{dG_1^*}{dt} = G_1 F_1(G_i) - \left(\gamma_{G,1} + \mu\right) G_1^*, \tag{B.1b}$$

where $F_3(G_i)$ and $F_1(G_i)$ are given in Eq. (2). We also assume the same dilution and degradation rates for the activated forms of the proteins as for the inactive forms.

- *Fractional transcriptional level*: Here, we describe the complete derivation of the function $\mathcal{R}_n$ presented in Eq. (4). Assuming that the dimerization reactions presented in Table B1 are at equilibrium, we can conclude that the dissociation constants of all relevant molecular species are given by the ratio $\frac{\text{Reactants}}{\text{Products}}$. Based on this, we can derive the following expressions for the dimer molecules $G_{80,d}$, $G_{3,d}^*$ and $G_{1,d}^*$:

$$K_{D,80} = \frac{G_{80}^2}{G_{80,d}} \Rightarrow G_{80,d} = \frac{G_{80}^2}{K_{D,80}} \tag{B.2a}$$

$$K_{D,3} = \frac{(G_3^*)^2}{G_{3,d}^*} \Rightarrow G_{3,d}^* = \frac{(G_3^*)^2}{K_{D,3}} \tag{B.2b}$$

$$K_{D,1} = \frac{(G_1^*)^2}{G_{1,d}^*} \Rightarrow G_{1,d}^* = \frac{(G_1^*)^2}{K_{D,1}}. \tag{B.2c}$$

It is also mentioned in Table B1 that the three dimers $G_{80,d}$, G_3^* and G_1^* have high affinities for the three promoter conformations, D_2, D_3 and D_4, respectively. Assuming that these quantities reach equilibrium quickly, we can write the reactions in terms of their dissociation constants. Using this result and Eqs. (B.2a–c), we can express the promoter conformations D_1, D_3 and D_4 in terms of D_2 as follows:

$$K_{B,80} = \frac{G_{80,d} D_1}{D_2} \Rightarrow D_1 = \frac{K_{B,80} D_2}{G_{80,d}} = \frac{K_{D,80} K_{B,80} D_2}{G_{80}^2} \tag{B.3a}$$

$$K_{B,3} = \frac{G_{3,d}^* D_2}{D_3} \Rightarrow D_3 = \frac{G_{3,d}^* D_2}{K_{B,3}} = \frac{(G_3^*)^2 D_2}{K_{D,3} K_{B,3}} \tag{B.3b}$$

$$K_{B,1} = \frac{G_{1,d}^* D_3}{G_{3,d}^* D_4} \Rightarrow D_4 = \frac{G_{1,d}^* D_3}{G_{3,d}^* K_{B,1}} = \frac{G_{1,d}^* G_{3,d}^* D_2}{G_{3,d}^* K_{B,1} K_{B,3}} = \frac{G_{1,d}^* D_2}{K_{B,1} K_{B,3}}. \tag{B.3c}$$

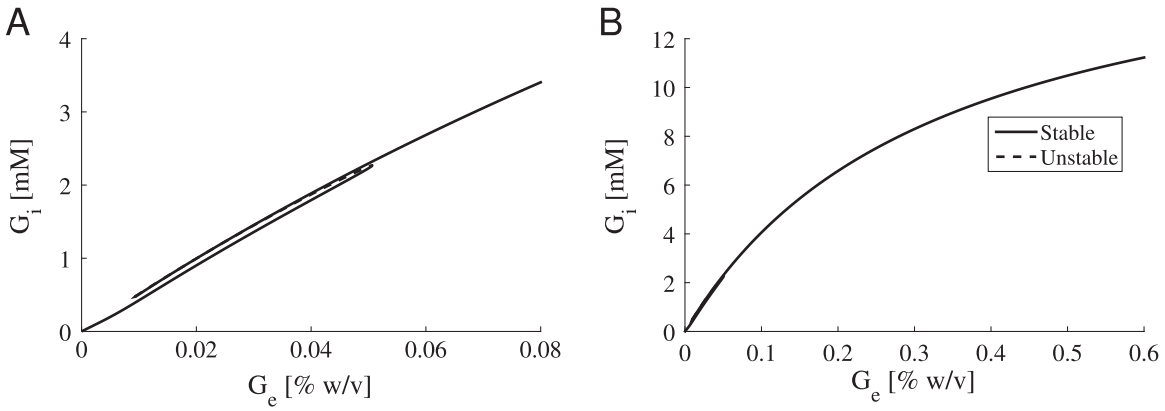

Fig. B1. One-parameter bifurcation with respect to the extracellular galactose concentration (G_e). The stable (solid) and unstable (dashed) branches of steady-state values of G_i within the range (A) [0,0.08]% w/v, and (B) [0,0.6]% w/v of galactose (G_e) as defined in Fig. 2. The choices in the G_e range were to focus on two important aspects: (1) the closeness of the two stable branches (in panel A), and (2) G_i levels with G_e saturation (in panel B). Due to the difference in time scales between the fast metabolic subsystem and the slow GAL regulon, the bistability is within a very narrow G_i range, compared to that of Fig. 2.

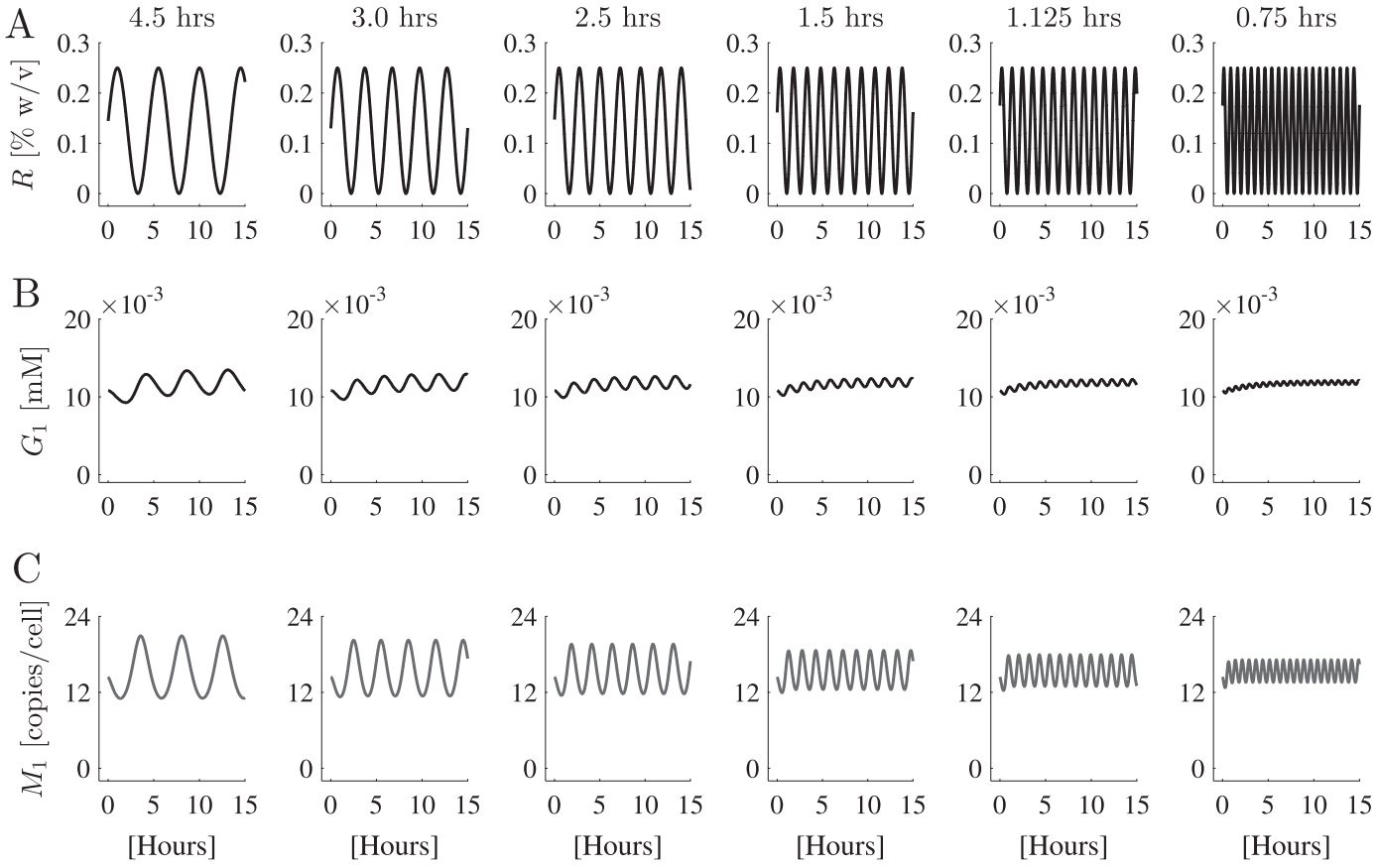

Fig. B2. Model response to oscillatory glucose input signal, generated using a GAL2 mutant cell. (A) The oscillatory glucose input signal applied with a period defined on top of each panel. (B) Gal1 output signal, generated from the extended 5D model, showing a similar 5 h period as that seen in Fig. 5(B). (C) GAL1 mRNA output signal, generated from the 9D model, showing a slightly lower baseline when compared to the wild-type strain of Fig. 5(C).

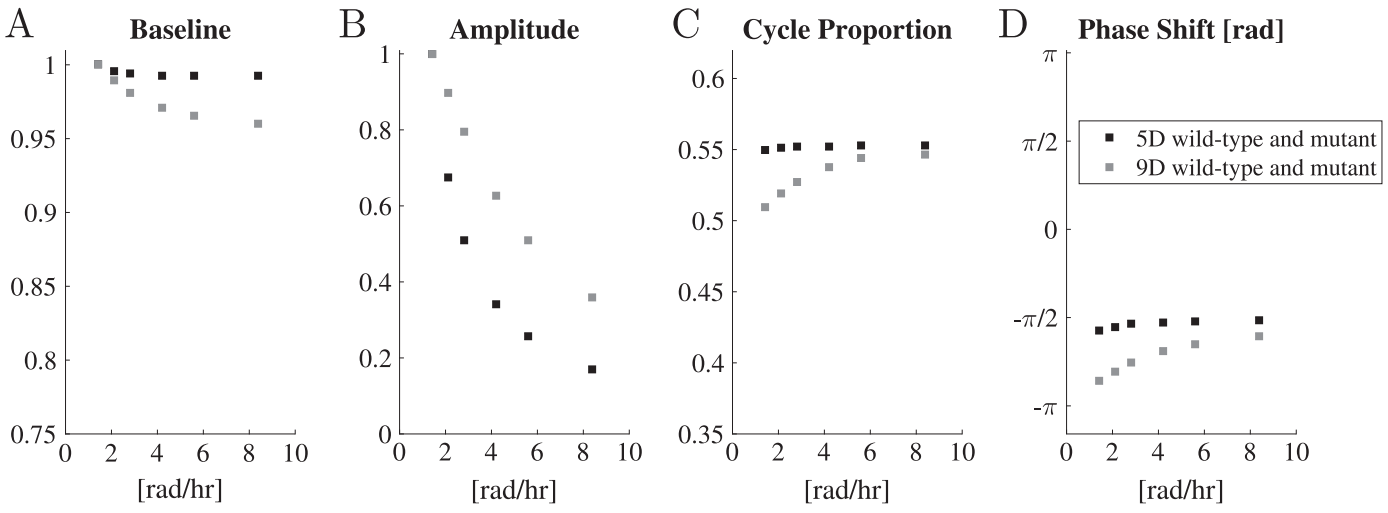

Fig. B3. Comparison between the properties of the G_1 oscillatory output signal in wild-type and GAL2 mutant strains, as determined by the numerical simulations of the 5D and 9D models in Figs. 5 and B2. The four characteristic measures defined in Table 4 are used; namely, the (A) baseline, (B) amplitude, (C) percentage of the upstroke, and (D) phase shift. Notice the minimal change in the phase shift.

These expressions are then used to formulate $\mathcal{R}_1$, the fractional transcriptional level for mRNA strains containing a single $[UAS]_g$,

$$\mathcal{R}_1 = \frac{D_1 + D_3 + D_4}{D_1 + D_2 + D_3 + D_4} = 1 - \frac{D_2}{D_1 + D_2 + D_3 + D_4},$$

or equivalently

$$\mathcal{R}_1(G_{80}, G_3^*, G_1^*) = 1 - \frac{1}{1 + \frac{K_{D,80}K_{B,80}}{G_{80}^2} + \frac{(G_3^*)^2}{K_{D,3}K_{B,3}} + \frac{(G_1^*)^2}{K_{D,1}K_{B,1}K_{B,3}}}.$$

As mentioned, GAL2 and GAL1 mRNAs contain 2 and 5 $[UAS]_g$, respectively, therefore the promoter can exist in more conformations than the four terms presented above. In this context, we simply need to multiply the kinetic reactions shown in Table B1

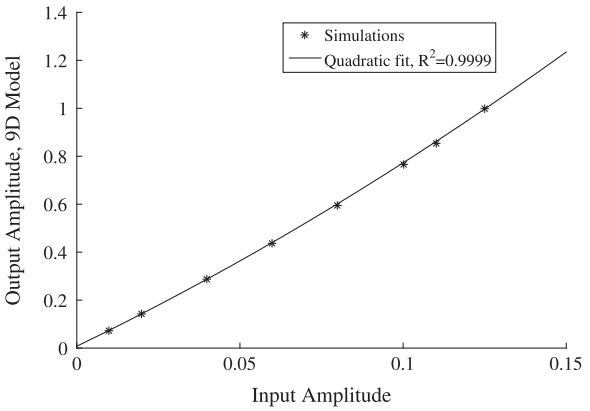

Fig. B4. The amplitude of the output signal M_1, generated by the 9D model, is plotted (as asterisks) against the amplitude of the glucose oscillatory input signal. The period of the glucose signal used here was 4.5 h. A quadratic polynomial (solid line) generated the best fit to numerical data, probably since the Gal regulatory proteins affecting the genetic branch of the network always appear in dimerized form.

below by the number of existing $[UAS]_g$ (n). This means that $\mathcal{R}_n$ is given by

$$\mathcal{R}_n(G_{80}, G_3^*, G_1^*) = 1 - \frac{1}{1 + \sum_{k=1}^{n}\left(\frac{\sqrt{K_{D,80}K_{B,80}}}{G_{80}}\right)^{2k} + \sum_{k=1}^{n}\left(\frac{G_3^*}{\sqrt{K_{D,3}K_{B,3}}}\right)^{2k} + \sum_{k=1}^{n}\left(\frac{G_1^*}{\sqrt{K_{D,1}K_{B,1}K_{B,3}}}\right)^{2k}}.$$

- *Quasi steady state of the Galactose-1-Phosphate*: Here, we present the derivation of the rate of change for intracellular galactose levels (G_i). This is done by applying QSS assumption on the rate of change of G_p (given by Eq. (16)) to obtain

$$(\delta + \mu)G_{p(ss)}^2 + (\delta + \mu)k_p(G_i)G_{p(ss)} - \sigma(G_i)G_iG_1 = 0,$$

where $G_{p,ss}$ represents the steady state value of Gal1P (G_p). Solving for $G_{p,ss}$ gives one single positive solution

$$G_{p(ss)} = \frac{-k_p(G_i) + \sqrt{k_p(G_i)^2 + \frac{4\sigma(G_i)G_iG_1}{\delta}}}{2}. \tag{B.4a}$$

The expression for $G_{p(ss)}$ can be substituted into Eq. (15) for the intracellular galactose.

B.2. Schematic representation of the kinetic reactions occurring at the level of the GAL mRNA promoter

See Table B1.

B.3. Additional results

- *Steady state behaviour of intracellular galactose*: We study the bifurcation behaviour of the system with respect to intracellular galactose (G_i). The goal is to determine how the steady state behaviour of G_i in the reduced 5D model depends on G_e and if bistability is maintained. Fig. B1(A) shows that the bifurcation diagram of G_i with respect to G_e, using the same range of [0, 0.08]% w/v of galactose as that used in Fig. 2, also exhibits bistability in the form of a switch. Indeed, the two stable branches of this bifurcation diagram are so close, they appear as one curve possessing a Hill-like profile that eventually plateaus at high values of G_e. The rate of change of G_i, according to the reduced model, depends on reactions that possess both slow and fast time scales. Due to the fast reactions taking place in the metabolic system (when compared to those in the GAL regulon), such as transport and phosphorylation, the bistable switch associated with G_i is not as pronounced as that for the proteins of Fig. 2. Thus verifying this switching behaviour at the

Table B1
Schematic representation of the kinetic reactions occurring at the level of the GAL mRNA promoter. The promoter conformations used in the "Description" are $D_1 = [UAS]_g$: $G_{4,d}$, $D_2 = [UAS]_g$: $G_{4,d}$: $G_{80,d}$, $D_3 = [UAS]_g$: $G_{4,d}$: $G_{80,d}$: $G_{3,d}^*$ and $D_4 = [UAS]_g$: $G_{4,d}$: $G_{80,d}$: $G_{1,d}^*$. K_{D_i}, $i \in \{80, 3, 1\}$ are the dissociation constants of the dimers into monomers, whereas $K_{B,i}$, $i \in \{8, 3, 1\}$ are the dissociation constants of the promoter conformations. $F_3(G_i)$ and $F_1(G_i)$ are activation rates for G_3 and G_1 molecules in the presence of galactose.

Energy source	Effect on the GAL network	Description	Process	Figure
Glucose	Repression	$[UAS]_g \rightarrow [UAS]_g: M_{1p}$	Mig1p protein binds to the upstream activating sequence ($[UAS]_g$) on the GAL genes and refrains the RNA polymerase from transcription	
Raffinose	Induction leakage	$[UAS]_g \rightarrow D_1$	G4 dimers ($[G_{4d}]$) bind to $[UAS]_g$ and allow transcription to occur	1(B)1
Raffinose, Galactose	Induction leakage	$G_{80} + G_{80} \xrightarrow{K_{D,80}} G_{80,d}$	G_{80} dimers ($[G_{80d}]$) bind to the previously formed complex. They inhibit Gal protein transcription, with some leakage for G_3 and G_{80}	
		$D_1 + G_{80,d} \xrightarrow{K_{B,80}} D_2$		1(B)2
Galactose	Early induction	$G_3 \xrightarrow{F_3(G_i)} G_3^*$	Galactose activates G_3 molecules, which dimerize. Upon dimerization, these molecules bind to the full complex and induce transcription of Gal proteins	
		$G_3^* + G_3^* \xrightarrow{K_{D,3}} G_{3,d}^*$		
		$D_2 + G_{3,d}^* \xrightarrow{K_{B,3}} D_3$		1(B)3
Galactose	Late induction	$G_1 \xrightarrow{F_1(G_i)} G_1^*$	Activated G_1 dimers replace G_3 dimers and transcription continues	
		$G_1^* + G_1^* \xrightarrow{K_{D,1}} G_{1,d}^*$		1(B)4
		$D_3 + G_{1,d}^* \xrightarrow{K_{B,1}} D_4 + G_{3,d}^*$		

level of intracellular galactose could be experimentally challenging.

Nonetheless, it is important to point out that the switching behaviour in Fig. B1 can occur for various reasons. The prominent change in stability occurring in the GAL network destabilizes the positive and the negative feedback elements of the system. Moreover, a change in the ratio between the transporter Gal2 and the enzyme Gal1, or a change in the concentration of the two activators, Gal1 and Gal3, could underlie this behaviour. As a result, we believe that bistability in the metabolic pathways of the GAL network occurs due to the inherent properties of the system at the gene regulation level. Based on the discussion above, the equilibrium concentration of G_i appears to reach a saturating level of 12 mM for high extracellular galactose levels ($\geq$0.6% w/v of G_e).

- Dynamics of the model simulation depicting the response of GAL2Δ strain to glucose oscillations.
- Quantification of the four measures defining the output response of the GAL network.
- Relation between the amplitude of the glucose input signal and the amplitude of the GAL network output signal.

Appendix C. Supplementary data

Supplementary data associated with this article can be found in the online version at http://dx.doi.org/10.1016/j.jtbi.2016.07.004.

References

Abramczyk, D., Holden, S., Page, C.J., Reece, R.J., 2012. Interplay of a ligand sensor and an enzyme in controlling expression of the *Saccharomyces cerevisiae* GAL genes. Eukaryot. Cell 11 (3), 334–342.

Acar, M., Becskei, A., van Oudenaarden, A., 2005. Enhancement of cellular memory by reducing stochastic transitions. Nature 435 (7039), 228–232.

Acar, M., Pando, B.F., Arnold, F.H., Elowitz, M.B., Van Oudenaarden, A., 2010. A general mechanism for network-dosage compensation in gene circuits. Science 329 (5999), 1656–1660.

Apostu, R., Mackey, M.C., 2012. Mathematical model of GAL regulon dynamics in *Saccharomyces cerevisiae*. J. Theor. Biol. 293, 219–235.

Arava, Y., Wang, Y., Storey, J.D., Liu, C.L., Brown, P.O., Herschlag, D., 2003. Genome-wide analysis of mRNA translation profiles in *Saccharomyces cerevisiae*. Proc. Natl. Acad. Sci. 100 (7), 3889–3894.

Barros, L.F., 1999. Measurement of sugar transport in single living cells. Pflüg. Arch. 437 (5), 763–770.

Bennett, M.R., Pang, W.L., Ostroff, N.A., Baumgartner, B.L., Nayak, S., Tsimring, L.S., Hasty, J., 2008. Metabolic gene regulation in a dynamically changing environment. Nature 454 (7208), 1119–1122.

Bhat, P.J., 2008. Galactose regulon of yeast. From Genetics to Systems Biology.

Bonven, B., Gulløv, K., 1979. Peptide chain elongation rate and ribosomal activity in Saccharomyces cerevisiae as a function of the growth rate. Mol. Gen. Genet. (MGG) 170 (2), 225–230.

de Atauri, P., Orrell, D., Ramsey, S., Bolouri, H., 2004. Evolution of design principles in biochemical networks. Syst. Biol. 1 (1), 28–40.

de Atauri, P., Orrell, D., Ramsey, S., Bolouri, H., 2005. Is the regulation of galactose 1-phosphate tuned against gene expression noise? Biochem. J. 387, 77–84.

de Jongh, W.A., Bro, C., Ostergaard, S., Regenberg, B., Olsson, L., Nielsen, J., 2008. The roles of galactitol, galactose 1-phosphate, and phosphoglucomutase in galactose-induced toxicity in *Saccharomyces cerevisiae*. Biotech. Bioeng. 101 (2), 317–326.

Ebel, W., 1985. Carrier facilitated diffusion. J. Math. Biol. 21 (3), 243–271.

Giniger, E., Varnum, S.M., Ptashne, M., 1985. Specific DNA binding of GAL4, a positive regulatory protein of yeast. Cell 40 (4), 767–774.

Gitzelmann, R., 1995. Galactose-1-phosphate in the pathophysiology of galactosemia. Eur. J. Pediatr. 154 (2), S45–S49.

Holstege, F.C., Jennings, E.G., Wyrick, J.J., Lee, T.I., Hengartner, C.J., Green, M.R., Golub, T.R., Lander, E.S., Young, R.A., 1998. Dissecting the regulatory circuitry of a eukaryotic genome. Cell 95 (5), 717–728.

Horak, J., Wolf, D.H., 1997. Catabolite inactivation of the galactose transporter in the yeast *Saccharomyces cerevisiae*: ubiquitination, endocytosis, and degradation in the vacuole. J. Bacteriol. 179 (5), 1541–1549.

Ideker, T., Thorsson, V., Ranish, J.A., Christmas, R., Buhler, J., Eng, J.K., Bumgarner, R., Goodlett, D.R., Aebersold, R., Hood, L., 2001. Integrated genomic and proteomic analyses of a systematically perturbed metabolic network. Science 292 (5518), 929–934.

Khadra, A., 2009. Synchrony due to parametric averaging in neurons coupled by a shared signal. Phys. D: Nonlinear Phenom. 238 (7), 771–781.

Kosterlitz, H., 1943. The fermentation of galactose and galactose 1-phosphate. Biochem. J. 37 (3), 322.

Lashkari, D.A., DeRisi, J.L., McCusker, J.H., Namath, A.F., Gentile, C., Hwang, S.Y., Brown, P.O., Davis, R.W., 1997. Yeast microarrays for genome wide parallel genetic and gene expression analysis. Proc. Natl. Acad. Sci. 94 (24), 13057–13062.

Lohr, D., Venkov, P., Zlatanova, J., 1995. Transcriptional regulation in the yeast GAL gene family: a complex genetic network. Fed. Am. Soc. Exp. Biol. (FASEB) J. 9 (9), 777–787.

Maier, A., Völker, B., Boles, E., Fuhrmann, G.F., 2002. Characterization of glucose transport in *Saccharomyces cerevisiae* with plasma membrane vesicles (countertransport) and intact cells (initial uptake) with single Hxt1, Hxt2, Hxt3, Hxt4, Hxt6, Hxt7 or Gal2 transporters. Fed. Eur. Microbiol. Soc. (FEMS)-Yeast Res. 2 (4), 539–550.

Melcher, K., Xu, H.E., 2001. Gal80-Gal80 interaction on adjacent Gal4p binding sites is required for complete GAL gene repression. Eur. Mol. Biol. Organ. (EMBO) J. 20 (4), 841–851.

Murphy, M., McHugh, B., Tighe, O., Mayne, P., O'Neill, C., Naughten, E., Croke, D.T., 1999. Genetic basis of transferase-deficient galactosaemia in Ireland and the population history of the Irish travellers. Eur. J. Hum. Genet. (EJHG) 7 (5), 549–554.

Ramos, J., Szkutnicka, K., Cirillo, V., 1989. Characteristics of galactose transport in *Saccharomyces cerevisiae* cells and reconstituted lipid vesicles. J. Bacteriol. 171 (6), 3539–3544.

Ramsey, S.A., Smith, J.J., Orrell, D., Marelli, M., Petersen, T.W., de Atauri, P., Bolouri, H., Aitchison, J.D., 2006. Dual feedback loops in the GAL regulon suppress cellular heterogeneity in yeast. Nat. Genet. 38 (9), 1082–1087.

Reifenberger, E., Boles, E., Ciriacy, M., 1997. Kinetic characterization of individual hexose transporters of *Saccharomyces cerevisiae* and their relation to the triggering mechanisms of glucose repression. Eur. J. Biochem. 245 (2), 324–333.

Reznik, E., Kaper, T.J., Segrè, D., 2013. The dynamics of hybrid metabolic-genetic oscillators. Chaos: Interdiscip. J. Nonlinear Sci. 23 (1), 013132.

Rogers, S., Holtzapple, P.G., Mellman, W.J., Segal, S., 1970. Characteristics of galactose 1-phosphate uridyl transferase in intestinal mucosa of normal and galactosemic humans. Metabolism 19 (9), 701–708.

Sellick, C.A., Campbell, R.N., Reece, R.J., 2008. Galactose metabolism in yeast-structure and regulation of the Leloir pathway enzymes and the genes encoding them. Int. Rev. Cell Mol. Biol. 269, 111–150.

Sherman, F., 2002. Getting started with yeast. Methods Enzymol. 350, 3–41.

Stockwell, S.R., Landry, C.R., Rifkin, S.A., 2015. The yeast galactose network as a quantitative model for cellular memory. Mol. BioSyst. 11 (1), 28–37.

Timson, D.J., 2006. The structural and molecular biology of type III galactosemia. Int. Union Biochem. Mol. Biol. (IUBMB)-Life 58 (2), 83–89.

Timson, D.J., 2007. Galactose metabolism in *Saccharomyces cerevisiae*. Dyn. Biochem. Process Biotechnol. Mol. Biol. 1 (1), 63–73.

Timson, D.J., Reece, R.J., 2002. Kinetic analysis of yeast galactokinase: implications for transcriptional activation of the GAL genes. Biochimie 84 (4), 265–272.

Tyson, C.B., Lord, P.G., Wheals, A.E., 1979. Dependency of size of *Saccharomyces cerevisiae* cells on growth rate. J. Bacteriol. 138 (1), 92–98.

van den Brink, J., Akeroyd, M., van der Hoeven, R., Pronk, J., De Winde, J., Daran-Lapujade, P., 2009. Energetic limits to metabolic flexibility: responses of Saccharomyces cerevisiae to glucose–galactose transitions. Microbiology 155 (4), 1340–1350.

Venkatesh, K., Bhat, P., Anand Kumar, R., Doshi, P., 1999. Quantitative model for Gal4p-mediated expression of the galactose/melibiose regulon in *Saccharomyces cerevisiae*. Biotechnol. Prog. 15 (1), 51–57.

Venturelli, O.S., El-Samad, H., Murray, R.M., 2012. Synergistic dual positive feedback loops established by molecular sequestration generate robust bimodal response. Proc. Natl. Acad. Sci. 109 (48), E3324–E3333.

Venturelli, O.S., Zuleta, I., Murray, R.M., El-Samad, H., 2015. Population diversification in a yeast metabolic program promotes anticipation of environmental shifts. PLoS Biol. 13 (1), e1002042.

Wang, Y., Liu, C.L., Storey, J.D., Tibshirani, R.J., Herschlag, D., Brown, P.O., 2002. Precision and functional specificity in mRNA decay. Proc. Natl. Acad. Sci. 99 (9), 5860–5865.